https://doi.org/10.5194/egusphere-2024-310
Preprint. Discussion started: 5 March 2024

Fifty-year seasonal variability of East African droughts and floods recorded in Central Afar lake sediments (Ethiopia) and their connections with ENSO

Carlo Mologni [1*], Marie Revel [1], Eric Chaumillon [2], Emmanuel Malet [3], Thibault Coulombier [2], Pierre Sabatier [3], Pierre Brigode [1], Gwenael Hervé [4], Anne-Lise Develle [3], Laure Schenini [1], Medhi Messous [1], Gourguen Davtian [6], Alain Carré, [6], Delphine Bosch [7], Natacha Volto [2], Clément Ménard [5], Lamya Khalidi [6], Fabien Arnaud [3]

[1] Université Côte d'Azur, CNRS, OCA, IRD, Geoazur, 250 rue Albert Einstein, 06500 Valbonne, France.
[2] University of La Rochelle, UMR CNRS 7266 LIENSs, La Rochelle, France.
[3] Environnement Dynamique et Territoire de Montagne (EDYTEM), CNRS, Université Savoie Mont-Blanc, Le Bourget du lac, France.
[4] Laboratoire des Sciences du Climat et de l'Environnement/IPSL, CEA, CNRS, UVSQ, University of Paris-Saclay, Gif-sur-Yvette, France.
[5] EPCC, Centre Européen de Préhistoire, Avenue Léon-Jean Grégory - 66720 – Tautavel, France
[6] Université Côte d'Azur, CNRS, CEPAM – UMR 7264, 24 av. des Diables Bleus 06300 Nice, France.
[7] Géosciences Montpellier, UMR-CNRS 5243, Université de Montpellier, 34095 Montpellier, France
*Corresponding author

Abstract

Understanding past and present hydro-system feedbacks to global ocean-atmospheric interactions represents one of the main challenges to preventing droughts, extreme events and related human catastrophes in the face of global warming, especially in arid and semiarid environments. In eastern Africa, the El Niño-Southern Oscillation (ENSO) was identified as one of the primary drivers of precipitation variability affecting water availability. However, the northern East African Rift System (EARS) still suffers from ENSO climate teleconnection and the underrepresentation of predictive models because of the scarcity of local-to-regional historical or palaeo-data.

In this paper, we provide a 50-year seasonal flood/drought chronicle of the Awash River catchment from the study of laminated sediment from Gemeri and Afambo lakes (Central Afar region, Ethiopia), with the aim of reconstructing the magnitude of regional hydro-climatic events. Pluri-centimetric micro-laminated lithogenic facies alternating with pluri-millimetric carbonate-enriched facies are investigated in both lakes. We couple dating methods including radiocarbon, short-lived radionuclides, palaeomagnetic field variations and varve counting on both lake deposits to build a high-resolution age model and to discuss the regional hydro-sedimentary dynamics of the Awash River over the last ~700 years, with a focus on the last fifty years.

Using a multiproxy approach, we observe that following a multi-centennial enhanced hydrological period, the two lakes experienced a gradual decrease in river load inflow since 1979 CE, attaining extreme drought and high evaporative conditions between 1991 and 1997 CE. In 2014, the construction of a dam and the improvement of agricultural hydraulic management in the lower Awash River plain impacted the erodibility of local soils and the hydro-sedimentary balance of the lake basins, as evidenced by a disproportionate sediment accumulation rate.

https://doi.org/10.5194/egusphere-2024-310
Preprint. Discussion started: 5 March 2024

Comparison of our quantitative reconstruction with i) lake water surface evolution expressed in Km^2, ii) the interannual Awash River flow rates expressed in mm/yr, and iii) the El Niño 3.4 model highlights the intermittent connections between ENSO SST anomalies, regional droughts and hydrological conditions in the northern EARS.

1 Introduction

According to the Sixth Assessment Report of the Intergovernmental Panel on Climate Change (IPCC), climate warming has been more rapid in Africa in recent decades than in any other region of the world (IPCC, 2022). Global climate projections further suggest that the Horn of Africa will experience strong disturbances of its usual hydrological cycle, with both increasing frequency of intense rainfall events leading to enhanced flash-flood hazards and a generalized scarcity of rainfall, leading to frequent severe drought episodes (Palmer et al., 2023). Such climatic instability may induce the collapse of the local food production system, leading to famine, as it occurred in the decades between 1970 and 1990 (FAO, 2000). More recently, the shorter-than-normal 2021 rainy season led to a 70% reduction in average precipitation compared with seasonal norms, which raised an international alert and mobilization for the mitigation of desertification processes in the Horn of Africa (FAO, 2022).

Facing such evidence, eastern Africa is currently the focus for understanding recent (Holocene scale) past climate dynamics (Lennard et al., 2018) to simulate future projections, support regional ecosystem sustainability (Niang et al., 2014) and reduce rural population vulnerability to climate warming (FAO, 2022). Palaeoclimatic reconstructions have long been used to understand past climate variability to build more robust future climatic models in Africa. Even if global climate and hydrological model simulations have made considerable progress, reconstructions or tendencies of future precipitation and atmospheric dynamics in eastern Africa - source of moisture fluxes from the Atlantic or Indian Oceans (Marzin and Braconnot, 2009) - which affect continental hydrology at the regional-to-local scale remain to be developed (Dosio et al., 2019; Lennard et al., 2018). Indeed, the lack of widespread regional-to-local palaeoclimatic data makes it difficult to establish regional climatic models and the link between global hydroclimate variability and the functioning of specific hydro-systems.

In East Africa, precipitation variability is influenced by multiple interactions between patterns of remote climate forcing, regional circulation and local geographic factors acting at local and global scales (Nicholson, 2017). At a wider scale, the El Niño-Southern Oscillation (ENSO) was identified as one of the primary drivers of precipitation in eastern Africa (Ficchì et al., 2021; Nicholson, 2017; Palmer et al., 2023). More research on regional and high-temporal resolution relationships between ENSO and flood/drought impacts in the present and in the past is increasingly needed (Ficchì et al., 2021; Ward et al., 2014). With the aim of filling this gap, this paper focuses on the acquisition of new hydro-sedimentary datasets (i.e., decennial to seasonal scale resolution) thanks to the study of lacustrine sedimentary sequences from one of the wider river catchments in the northern East African Rift System (EARS), namely the Awash River basin (Fig. 1).

https://doi.org/10.5194/egusphere-2024-310
Preprint. Discussion started: 5 March 2024

As flood occurrence and magnitude of the Awash River are mainly linked to fluctuation of the Ethiopian Highland precipitation regime over time, the establishment of regional flood chronicles from natural archives is key to evaluating the evolution of precipitation variability on land (Ficchì et al., 2021; Mologni et al., 2020; Wilhelm et al., 2022). Of all of the natural archives for hydrological reconstruction, lakes are privileged because they act as natural sinks, continuously trapping erosion products from an entire catchment over a long period (Sabatier et al., 2022; Wilhelm et al., 2018). Indeed, during flood events, water-transported detrital particles (or sediment discharge) are deposited on the lake bottom in the form of graded layers that differ from the intra-lake sedimentation related to lake productivity. Thus, lake sedimentary deposits are valuable to fully understand the relationships between hydroclimate, rainfall, floods, droughts and lake water conditions at the regional scale.

This paper presents the results from a multiproxy study combining a seismic survey with sedimentological and geochemical analyses performed on archives from the Afambo and Gemeri lakes located in the Abhe lake basin (Central Afar Region, Ethiopia, Fig. 1). The main objective of this study is to quantify variations of long-term Awash solid sedimentary discharges to establish regional flood activity and to reconstitute the hydrological regime of the Awash River. Moreover, human activities can also play a key role in sediment availability, which is a function of soil erodibility and transport processes (Arnaud et al., 2016; Arnaud and Sabatier, 2022; Bajard et al., 2017, 2016; Syvitski et al., 2022). We aim first to identify the hydro-sedimentary processes in the Afambo and Gemeri Lake basins (Central Afar Region, Ethiopia) under human and hydroclimate/meteorological forcing over the long-term. Finally, we compare these flood and drought chronicles with global ENSO records and discuss the interaction between atmospheric anomalies, droughts and hydrological conditions in the northern EARS.

2 Study site: hydrological and geomorphological settings

2.1 Regional hydroclimatic patterns

The Abhe Lake basin, located at the northern extremity of the EARS (~12° N), is the widest and longest rifting-controlled sedimentary basin of the Afar Rift System (Fig. 1A). It corresponds to the topographic depression of the lower Awash valley (Fig. 1B) consisting of an area of 6 000 km^2 (Mologni et al., 2021). The Central Afar Region is currently a desert receiving ~400 mm/yr of local precipitation (Fig. 1D) with a mean annual evapotranspiration of ~2000 mm/yr (Fig. 1E). In such a dry context, the permanency of waterbodies such as lakes Gemeri and Afambo (Fig. 1C) is mainly supported by their hydrological dependence on permanent Awash River water supplies originating in the Ethiopian highlands (mean annual precipitation ~1000 mm/yr; Fig. 1D), whereby the hydrological regime is dominated by seasonal rainfall pertaining to the southwest African monsoon. With a drainage basin surface of over 112,700 km^2, the Awash River has an annual runoff of 4.6 BM^3. However, 72% of it is lost to evapotranspiration in the lowlands (Taddese et al., 2010).

https://doi.org/10.5194/egusphere-2024-310
Preprint. Discussion started: 5 March 2024

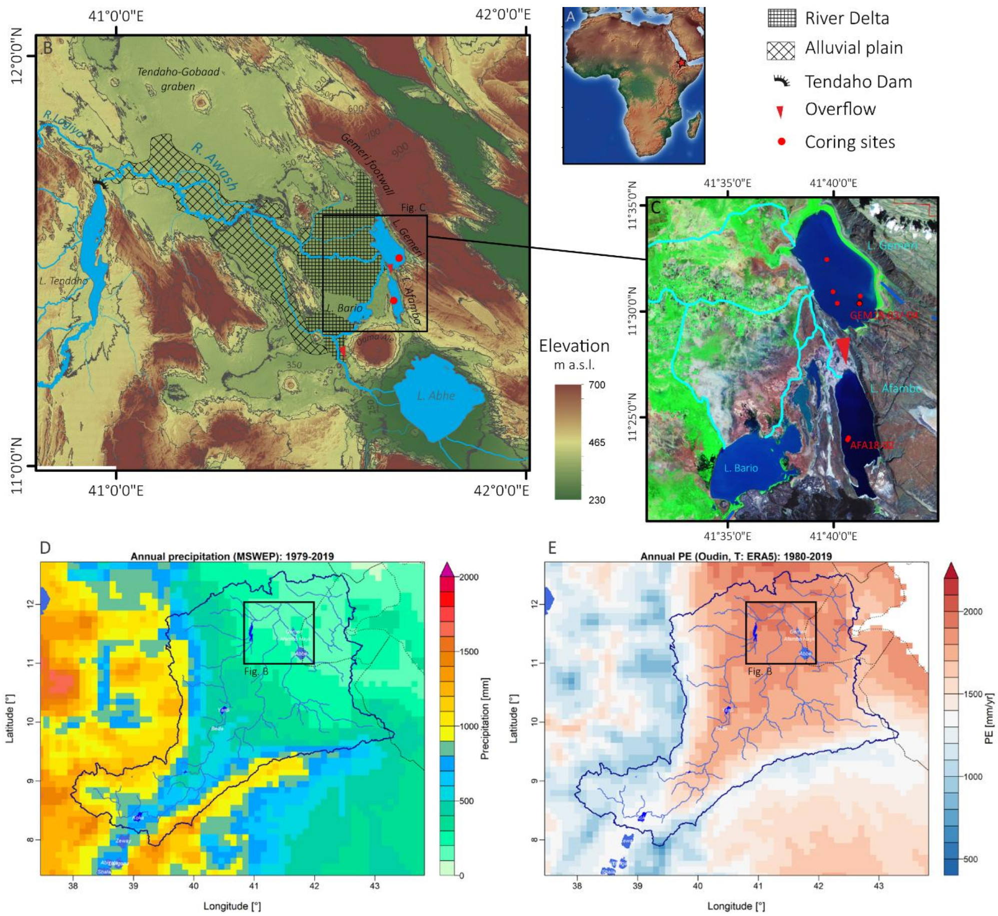

Figure 1*: Geographical, geomorphological and hydrological contexts of the study area and coring sites.* ***A****) Location of the Central Afar Region on a topographic map of Africa (red star);* ***B****) DEM of the Lake Abhe basin (SRTM) corresponding to the Lower Awash Valley with the location of Gemeri, Afambo and Abhe waterbodies, the corresponding alluvial plain and the Awash River delta, the main coring sites (red dots), the overflow directions and the Tendaho dam;* ***C****) Focus on Lakes Afambo and Gemeri study sites with the location of coring sites (red dots), the local hydrographic network (light blue lines) and the overflow direction between the waterbodies;* ***D****) mean annual precipitation over the Awash River and Lake Abhe basins estimated over the 1979-2019 period using the MSWEP dataset Beck et al. (2019).* ***E****) Mean annual potential evapotranspiration over the Awash River and Lake Abhe basins estimated using the Oudin et al. (2005) formula and the air temperature of the ERA5 dataset Hersbach et al. (2020).*

When it feeds into Lakes Gemeri and Afambo Lakes, the Awash River has only crossed recent geological formations subsequent to the formation of the Oligocene Ethiopian basaltic trap flows. The lower Awash Valley is mainly composed of stratoid basalts formed between 4 and 0.4 Ma (Awaleh et al., 2016, Barberi and Varet, 1977; Varet, 2018) and intra-graben Quaternary accumulations, which still belong mainly to the Stratoid series group.

https://doi.org/10.5194/egusphere-2024-310
Preprint. Discussion started: 5 March 2024

2.2 Local geomorphological context

The northern part of the Lake Abhe basin is composed of an alluvial plain corresponding to irrigated agricultural fields and extended anthropogenic water channels, and a lobate delta in its lower part (Fig. 1b). The remaining edges of the basin are composed of desert plains and basaltic/rhyolitic outcrops that constitute the Tendaho-Gobaad graben horsts (Fig. 1b). The delta fan spreads ~60 km from the northern Gemeri footwall fault through the Gemeri and Bario waterbodies until the Dama Ale volcano slopes to the south (Fig. 1b).

The Awash freshwater supplies first reach Lake Gemeri (11°51'N, 41°69' E), and overflowing into Lake Afambo (11° 40' N, 41° 68' E). In contrast to Gemeri, Lake Afambo is not located on the delta fan and does not possess any aerial estuary (Fig. 1B, C). Indeed, Afambo Lake is reached during the dry season by a single water channel and is permanently separated from the deltaic swamps by north-south basaltic outcrops (Fig. 1c, 2a). The rest of the Awash water supply is drained by the delta to the Bario waterbody and to the terminal river channel that flows down to Lake Abhe (Fig. 1B, C).

The local hydrological network led us to select two complementary coring sites for this study: Lake Gemeri, which borders the prodeltaic zone, mostly records the sedimentary signal from fluvial dynamics (Awash River solid load), and Lake Afambo, which is partially disconnected from deltaic dynamics, has the potential to record fine-grained sediment inputs, lacustrine primary productivity processes and to preserve the sedimentary record from hiatuses due to deltaic erosional dynamics.

The hydrological network of the Lower Awash River plain has been modified by the building of a dam for the agricultural development of this area conducted by the "*Tendaho Dam and Irrigation Project*" (Dereje et al., 2018; Kidane et al., 2014). The dam is located upon entry of the Awash River waters into the Lake Abhe basin area (Fig. 1b). The construction project began in 2010, and the dam started working in early 2014. Such massive infrastructure has led to the formation of the Tendaho artificial lake (Fig. 1b) and the current network of irrigation channels in the alluvial plain.

3 Materials and methods

3.1 Analysis of the water surface evolution of Lake Gemeri from satellite images (1984 – 2019)

We conducted imagery analyses of the water surfaces of Lakes Gemeri and Afambo from 1984 to 2021. We used the "Global Surface Water" dataset from the Copernicus Programme, which was generated using 4,716,475 scenes from Landsat 5, 7, and 8 acquired between March 1984 and December 2021 by Landsat satellites provided by the USGS and NASA. The dataset contains maps of the location and temporal distribution of surface water from 1984 to 2021 at 30 m resolution and provides statistics on the extent and change of those water surfaces. For more information, refer to the associated journal

https://doi.org/10.5194/egusphere-2024-310
Preprint. Discussion started: 5 March 2024

article by Pekel et al. (2016). From this dataset, we computed statistics about the extent and change of the water surfaces. Using Envi software, version 5.4, we created a Meta image with the 37 water surface maps from 1985 to 2021 and generated statistics for the Meta image, which were then exported. However, for the years 1988, 1989, 1990, 1992, 1993, 1996, and 1997, the "Global Surface Water" dataset algorithm failed to concretely calculate the water surfaces, resulting in imprecise or missing data. As a result, we employed the quality assessment (QA) band in Landsat 5 images, which provides information on features such as clouds, shadows, ice, bare land, and water. Classification algorithms were applied to assign binary values to bits in the QA band based on pixel characteristics. By importing archives from the USGS and utilizing the Pixel_QA band associated with the available images, a water mask was created. This water mask allowed us to perform zonal statistics using ArcGIS Pro 3.0.3.

3.2 Seismic survey

In December 2018, a seismic reflection survey was conducted in the southernmost part of Lake Gemeri with the aim of exploring the internal architecture of the lake sedimentary fill and choosing the location of the coring site. The acquisition of 12 seismic profiles of Lake Gemeri (Fig. S1, S2) was performed using an IxBlue ECHOES 5000 CHIRP echo-sounder (LIENSs laboratory, La Rochelle, France). Chirp frequency band 2000 - 8000 Hz was selected, with a chirp length of 50 ms. Chirp data processing included auto grain control, time varying gain, staking of adjacent traces, and swell filtering.

3.3 Coring of Gemeri and Afambo Lakes

In December 2018, 10 short sedimentary cores were retrieved from Lakes Gemeri and Afambo during the CLIMAFAR 2018 survey. Shorter cores were retrieved using a UWITEC gravity corer, while a homemade modified Nesje-like corer permitted us to reach slightly more than 2 m sediment depth in Lake Gemeri (Fig. 1c). Details about the coring operations can be found on the French National Cybercatheque (https://cybercarotheque.fr/index.php?ope=530).
We focused the present study on cores collected in the deepest part of each lake, i.e., GEM18-03 (length 144 cm, IGSN number TOAE0000000354) and GEM18-04 (209 cm, IGSN number: TOAE0000000356) taken at 6 m water depth in Lake Gemeri, and AFA18-02 (173 cm, IGSN number TOAE0000000348) taken in Lake Afambo at 18 m water depth. GEM18-04 was cut into two parts in the field, and only the deepest part (109-209 cm below lake floor) of the overlapping core GEM18-03, was studied here. Core sections were split length-wise, photographed at high resolution, and described and logged in detail using the Munsell colour chart at the EDYTEM sedimentary lab facility. The identification of specific layers on the overlapping sections GEM18-03 and GEM18-04B together with the comparison of XRF core scanner and magnetic susceptibility signals led us to propose a 2.2 m long composite sediment sequence from Lake Gemeri, hereafter called GEM18-03/04.

https://doi.org/10.5194/egusphere-2024-310
Preprint. Discussion started: 5 March 2024

3.4 Analytical methods

3.4.1 XRF core scanner on soft sediments, ICP–MS measurements and clay mineralogy

To characterize the variation in major elements throughout cores GEM18-03/04 and AFA18-02, we performed non-destructive X-ray fluorescence (XRF) geochemical analyses on an AVAATECH Core Scanner at the EDYTEM laboratory (CNRS-Université de Savoie Mont-Blanc, France). The XRF analyses were performed following a 1 mm sampling step for the AFA18-02 section A, 2 mm for the lower section B (live time = 20s), and 5 mm for the GEM18-03/04 core. At each step, two successive measurements were performed at 10 kV (0.12mA) and 30 kV (0.15mA) voltages to assess the contribution of lighter (Al, Si, S, K, Ca, Ti, Mn, Fe) and heavier (Br, Sr, Rb, Zr, Pb) elements, respectively. Each individual power spectrum was transformed by deconvolution into relative contents of each computed element expressed in counts per second (cps). XRF data were subsequently transformed with a Centred Log-Ratio transformation package on R© software, with the aim of circumventing problems associated with matrix effects (e.g., variable water content and grain-size distribution) and irregularities of the core surface (Weltje and Tjallingii, 2008).

Principal component analysis (PCA) was performed on the XRF results using R® software (Sup. Mat. C) with the aim of characterizing the main geochemical signatures of particles composing the GEM18-03/04 and AFA18-02 sediments.

Major and trace element analyses were performed with a Quadrupole ICP–MS (AETE-ISO platform, Geosciences Montpellier, France) on 500 mg of powdered and homogenized sediment sample for 6 discrete samples in the GEM18-03/04 core and 11 discrete samples from the AFA18-02 core (Rauch et al., 2006).

X-ray diffraction analyses on clay minerals were performed on 5 samples from the GEM18-03/-04 sequence at the LHyGS laboratory CNRS-UMR7517 (Strasbourg, France) (Sup. Mat. F). Sediments were treated with HCl (10%) solution to avoid any carbonate content. Suspended clay fractions were separated following the procedure in Jackson (2005) and mounted on thin sections for oriented clay XRD analyses. With the aim of acquiring the whole diffraction spectrum, four diffractograms were obtained using a D8-Advance-Eco machine from the same sample with normal treatment, ethylene-glycol treatment, hydrazine treatment, and heat treatment for 4 h at 490°C. The semiquantitative content of clay minerals (%) was obtained from MacDiff version 4.1.2 software as a 2q° counts per second (cps) spectrum area measurement.

3.4.2 Sedimentological analyses

Grain-size analyses were performed at the Geoazur laboratory using a Coulter-LS2000 with a size range between 0.005 µm and 3775 µm. The analysis was performed following a 2.5 mm sampling step for the AFA18-02 core. We determined the grain size of the intercepts for 10%, 50% and 90% of the cumulative grain size curves (named Q90, Q50 and Q10 values; Folk and Ward, 1957). We use the coarsest fraction

(Q90) to characterize the deposit energy and to propose a hydrodynamic interpretation as suggested by Wilhelm et al., (2018).

Optical microscopic analyses were focused on 8 thin sections (10 x 2 cm) sampled from the AFA18-02 sequence and processed at the litho-preparation facilities of the EDYTEM laboratory (Arnaud and Sabatier, 2022). Microscopic observations were obtained on a Leica DM4 P at the Geoazur Laboratory at 25x and 1000x magnification using plane-polarized (PPL), crossed-polarized (XPL) and oblique incident (OIL) lights.

3.4.3 Chronology of Gemeri and Afambo Lake sequences

On the GEM18-03/04 sediment sequence, we combined short-lived radionuclides, ^{14}C measurements and palaeomagnetic analyses to build a reliable age-depth model along the 2.2 m of the composite section. A continuous sampling step of 6 cm was applied over the uppermost 66 cm of GEM18 to determine ^{210}Pb, ^{226}Ra and ^{137}Cs activities using well-type germanium detectors (SAGe Well) located below 1700 m of rocks at the "laboratoire souterrain de Modane" (CNRS-Université Grenoble Alpes) to reduce the influence of cosmic rays on gamma measurements (Reyss et al., 1995). Radionuclide-based age models were computed using the *serac* R package (Bruel and Sabatier, 2020). ^{14}C measurements were performed on 9 bulk organic matter and 4 shell samples (Sup. Mat. I, Fig. S23) using the ARTEMIS accelerator mass spectrometry (AMS) facility at the LSCE-LMC14 laboratory (Gif-sur-Yvette, France).

Palaeomagnetic measurements were performed on the entirety of the GEM18-03/-04 composite section. The principle of the palaeomagnetic method is to compare the declination, inclination and relative palaeointensity (RPI) records from the dated core with a reference curve of the secular variations in the geomagnetic field (Crouzet et al., 2019; Haberzettl et al., 2019; Li et al., 2021; Ólafsdóttir et al., 2013). Measurements were performed at the LSCE on u-channels sampled from the center of the GEM18-03 and GEM18-04B half cores. The direction of the characteristic remnant magnetization (ChRM), assumed to be a detrital remnant magnetization (DRM) acquired during the deposition of the sediment, was determined after alternating field (AF) demagnetization. The rock magnetic properties were investigated on u-channels from measurements of low-field susceptibility, acquisition and demagnetization of ARM and IRM, coupled to thermomagnetic, hysteresis curves and first order reversal curves (FORC) on 9 discrete samples. The full protocol is detailed in the supplementary material (Sup. Mat. D).

The age depth model of the AFA18-02 sequence was constrained by a combination of short-lived radionuclides, ^{14}C measurements and seasonal varve/laminae counting along the core sequence. A continuous sampling step of 10 cm was applied over 173 cm of the AFA18-02 sequence to determine ^{210}Pb, ^{226}Ra and ^{137}Cs activities. The ^{14}C measurements were performed on 9 organic matter samples at the ARTEMIS facility, including 2 vegetal macro-remains and 2 fish bone samples using ECHoMICHADAS, the MIcro Carbon Dating System of the LSCE laboratory (Table 1).

https://doi.org/10.5194/egusphere-2024-310
Preprint. Discussion started: 5 March 2024

3.5 Rainfall-runoff modelling

Observed streamflow time series at Tendaho Lake were extracted as daily timesteps from the GRDC dataset (*station ID: 1577603, 11.683 N, 40.950 E, catchment area: 62 088 km², owner of original data: Ethiopia - Ministry of Water Resources, Hydrology Department*). This time series is only available for the 1990-2004 period, with numerous missing data during the 1994-1996 and the 2003-2004 periods. To extend the temporal extension of the streamflow series, a rainfall-runoff model was used. The monthly rainfall-runoff model GR2M (Mouelhi et al., 2006) was used using the airGR R package (Coron et al., 2022, 2017). This conceptual and lumped model needs two continuous climatic time series as inputs, precipitation (P) and potential evapotranspiration (E). GR2M has two parameters that need to be calibrated for each studied catchment (cf. model diagram in Supp Mat. B, Fig. S3). The NOAA 20CR (v3, Slivinski et al., 2019) climatic reanalysis was extracted over the Awash River catchment at Tendaho Lake to generate a monthly time series of precipitation and air temperature over the 1836-2015 period. A monthly potential evapotranspiration time series was then estimated using the 20CR air temperature time series and the Oudin et al. (2005) formula. The model parameters were automatically calibrated using the Nash and Sutcliffe (1970) objective function over the 1990-2014 period, with an initialization of the model reservoirs during the 1980-1989 period. Finally, the GR2M model parameters obtained for the Awash River at Tendaho Lake were used over the 1836-2015 period to simulate streamflow over this period.

4 Results

4.1 Seismic reflection imagery on Lake Gemeri

Our chirp profiles provide a display of the bathymetry of Lake Gemeri for the first time. The average measured water depth is 3 m with a maximum of 6 m in the southern part of the lake. Afambo Lake is deeper, with a maximum depth of 18 m. The shallow depth (3 m on average) and very gentle slope of Lake Gemeri are consistent with its location in the prodeltaic area of the Awash Plain.

Unfortunately, seismic penetration in Lake Gemeri is reduced to a few decimetres. Within the central and eastern parts of the lake, an approximately 80 cm-thick upper sheet drape unit lies on a low-amplitude reflector parallel to the lake bottom (profile 006, Fig. 2b). On the western part of the Gemeri Lake, the upper sheet drape unit lies on a relatively strong amplitude reflector displaying a succession of small highs and lows (few meters to tens of meters wide and a few decimetres deep) showing the morphology of an erosional surface (profile 009, Fig. 2c). The succession of highs and lows along this erosional surface correspond to small channels indicating periods of drying of the lake. Below these reflectors, an extensive acoustic turbidity facies showing similarities with gassy facies (Bertin and Chaumillon, 2005; Garcia-Gil et al., 2002) is observed. Five measurements of total organic carbon from core GEM18-03 on 2 m of sediment indicate values of approximately 8.5% (Sup. Mat. E), which

https://doi.org/10.5194/egusphere-2024-310
Preprint. Discussion started: 5 March 2024

suggests that the gas could have come from the decomposition of organic matter (algae or upper vegetation) in the lake. The presence of gas in the Lake Gemeri sediment is likely, given the high organic productivity in this lake and the high content in organic matter in the sampled sediments and sequestration of organic matter that often occurs in anoxic fine sediments (Bertin and Chaumillon, 2005; Garcia-Gil et al., 2002; Roussel et al., 2009).

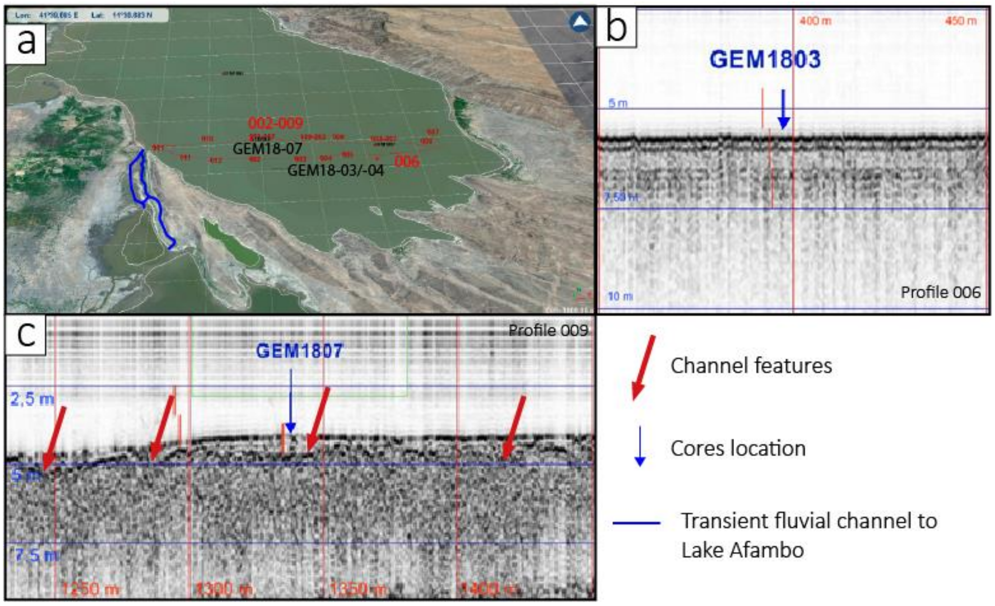

***Figure 2**: Seismic reflection imagery on Lake Gemeri: **a**) 3D satellite image projection of southern Lake Gemeri (LANDSAT) with the location of the seismic profiles and of the cores reported in Figs. b and c; **b**) 006 seismic profile with the location of GEM18-03 core (blue arrow); **c**) 009 seismic profile with the location of GEM18-07 core (blue arrow) and of channel features (red arrows).*

4.2 Sedimentology and geochemistry results

4.2.1 AFA18-02

The 173 cm-long sediment of AFA18-02 consists of undisturbed laminated sediments showing a clay-silty texture (Fig. 3a.1). A median size of 3 and 7 µm was measured at 2 mm resolution along the 173 cm of the core, indicating that the lake's sedimentation did not record any extreme coarse or erosional event (Fig. 3a.5). Along the core, the first striking characteristic of this sequence is the succession of a couple of distinct facies systematically composed of brownish-grey coloured pluri-centimetric layers (Facies-1; F1) alternating with orange/brown coloured pluri-millimetric layers (Facies-2; F2) and sometimes associated with millimetric white beds (Facies-3; F3, Fig. 3a.1, 4b.1). Thirty-two couplets were hence identified, over the entire 173 cm sediment sequence.

The major element distribution measured for 11 discrete samples (Tab. 1) indicates SiO_2 values oscillating between 25 and 46%, TiO_2 values between 0.7 and 1.7% and a high concentration in iron of

https://doi.org/10.5194/egusphere-2024-310
Preprint. Discussion started: 5 March 2024

approximately 8%. Carbonate content values oscillate between 6 and 24% (Tab. 1). From the discrete samples, the coefficient of correlation between Ca and Sr is $R^2 = 0.97$. This suggests that the source of the carbonaceous component does not change along the 173 cm. Thanks to PCA analyses, 3 geochemical end members from Dim.1 (53,67%)/Dim.2 (23,43%) were differentiated (Fig. S4): The first one (EM1) yields major elements Al, Si, Fe, Ti, K, Zr and Mn with high positive loading on Dim1. The second end-member (EM2) gathers elements composing carbonates (Ca and Sr) and elements involved in the evaporitic succession of minerals (S, Mg, Na) with high positive loading on Dim2 and positive loading on Dim1. The third end-member (EM3) includes only Br negative loading on Dim1 and Dim2, which is often used as a proxy for autochthonous organic matter in lakes (Bajard et al., 2016; Lefebvre et al., 2021). The PCA factor map ascribes F1 layers into the EM1 area and the F2/F3 layers into the EM2 area (Fig. S5). Consequently, we selected Ti, Sr, and Ca to geochemically characterize the F1 and F2/F3 facies. A good plot correlation between CLR transform XRF and ICP–MS measured elemental values (Fig. 3b) provides reliable Sr and Ca XRF data to geochemically characterize the three different sedimentary facies along the core sequence. F1 is composed of microlaminated clays enriched in Ti, Si and Fe elements (Fig. 3b.3). The F1 thickness varies substantially along the core, with an average thickness of ~3 cm between 173 and 137 cm, a thickness of ~1 cm between 137 and 120 cm, a thickness of 3.5 cm between 120 and 80 cm, and a thickness of ~9 cm between 80 and 0 cm. F2 (0.5-1 cm thickness) is composed of microlaminated clay, diffused secondary carbonate impregnations (sparite) and sporadic Fe-Mn nodules. Geochemically, the F2 layers are slightly enriched in Ca and Sr elements (Fig. 3a, 3b). F3 (0.3-0.5 cm thickness) is composed of a massive-to-microlaminated micritic/sparitic matrix (Fig. 7b.1) strongly enriched in Ca and Sr elements (Fig. 3a, 3b).

https://doi.org/10.5194/egusphere-2024-310
Preprint. Discussion started: 5 March 2024

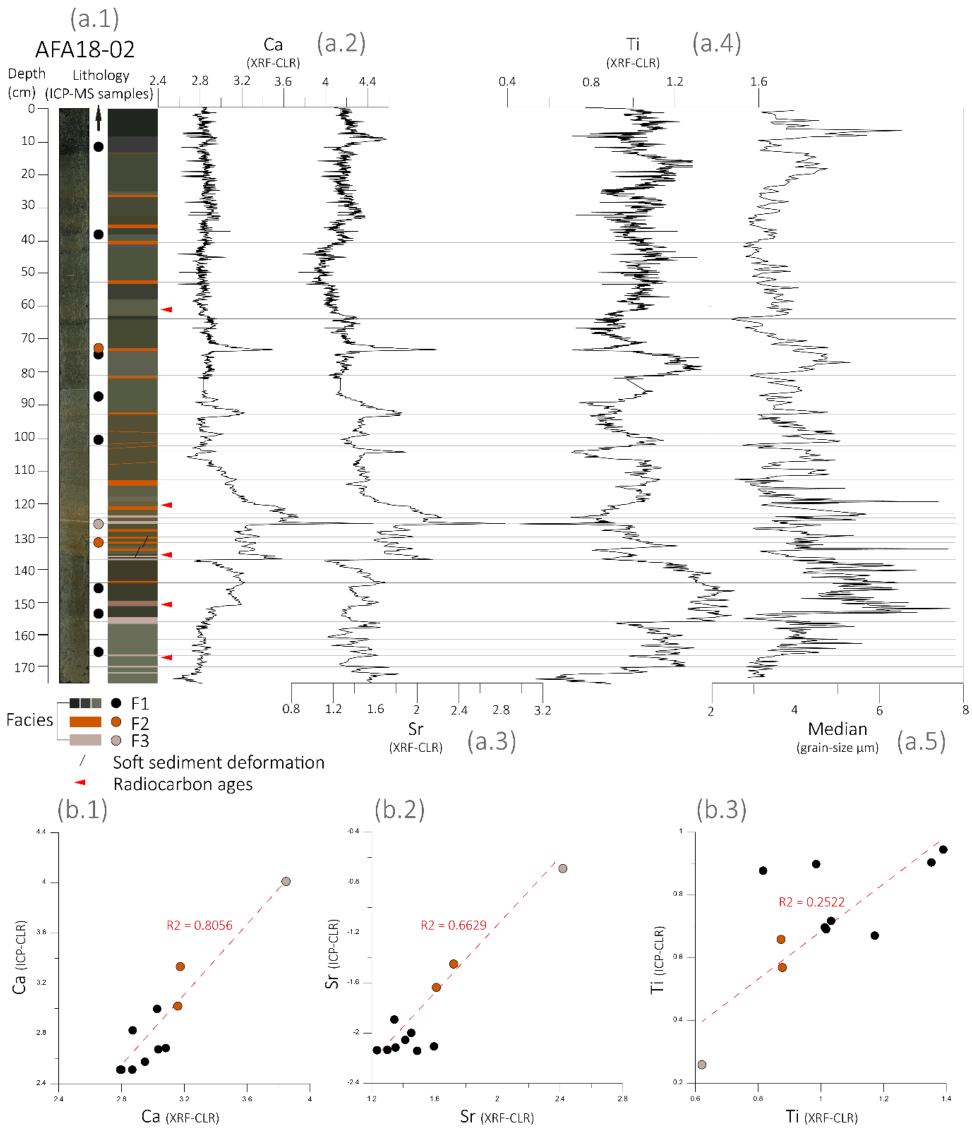

Figure 3: *Geochemical (XRF and ICP-MS) and sedimentological results on AFA18-02 core:* ***a.1****) Picture and lithology with the location of the sampling areas for ICP-MS analyses (dots);* ***a.2****) Ca XRF-(CLR) values;* ***a.3****) Sr XRF-(CLR) values;* ***a.4)*** *Ti XRF-(CLR) values;* ***a.5****) Grain size median;* ***b.1****) Correlation plot between Ca XRF-(CLR) and ICP-MS-(CLR) values;* ***b.2****) Correlation plot between Sr XRF-(CLR) and ICP-MS-(CLR) values;* ***b.3****) Correlation plot between Ti XRF-(CLR) and ICP-MS-(CLR) values.*

Grain size distributions indicate three general dominant modes, one sorted clay mode at approximately 1 to 2 µm, one well-sorted mode at approximately 19 µm, and the third is less dominant and lies in the sortable silt range at approximately 50 µm (Fig. 4b.3).

F1 layers present pronounced 1-2 µm and 50 µm modes, with the second represented mode at 19 µm. F2 and F3 are well sorted at approximately 40 and 126 cm.

https://doi.org/10.5194/egusphere-2024-310
Preprint. Discussion started: 5 March 2024

Dept (cm)	F	Na2O	MgO	Al2O3	K2O	CaO	TiO2	MnO	P2O5	SiO2	Fe2O3 (T)	Cr	Ni	Ba	Zr	Sr
		%	%	%	%	%	%	%	%	%	%	ppm	ppm	ppm	ppm	ppm
12	F1	1,97	4,62	13,13	1,85	6,30	1,50	0,10	0,28	45,80	9,57				271,65	423,40
39	F1	1,69	4,44	12,79	1,83	6,27	1,21	0,11	0,28	43,42	8,67	71,83	70,30	306,67	266,19	430,11
72	F2	1,32	4,35	10,60	1,43	14,16	1,06	0,11	0,26	36,48	7,30	59,87	56,34	371,84	221,51	847,12
73	F1	1,61	4,17	12,55	1,83	7,51	1,48	0,12	0,27	42,86	8,73	72,51	61,19	319,30	268,68	450,51
90	F1	1,39	4,08	11,78	1,92	8,37	1,14	0,10	0,26	42,62	8,26	72,86	62,70	287,74	254,22	480,19
100	F1	0,69	3,34	12,12	1,47	9,47	1,13	0,17	0,26	41,62	8,21	71,16	66,15	300,95	247,09	397,81
127	F3	0,96	5,28	6,67	1,01	23,79	0,67	0,14	0,19	25,11	4,57	39,57	40,49	399,08	136,28	1545,29
132	F2	1,34	4,93	10,58	1,53	10,39	1,24	0,11	0,25	37,96	7,42	67,73	62,20	351,79	227,72	706,21
148	F1	1,65	4,18	12,78	1,86	8,08	1,69	0,14	0,28	43,70	8,89	83,73	65,71	367,12	263,87	505,26
152	F1	1,58	4,47	12,64	1,89	6,93	1,55	0,12	0,26	43,45	8,82	82,59	63,67	329,38	266,35	454,91
168	F1	1,38	5,81	11,69	1,78	5,99	1,13	0,10	0,23	41,84	7,80	69,70	63,29	285,02	246,98	523,07

Tab 1*: Major and trace element concentrations of the AFA18-02 core.*

4.2.2 GEM18-03/04

The sediment of GEM18-03/04 is homogeneously clayey (Q50 = ~2.4 µm) and dark brown in colour (Fig. 5) all along its 220 cm. The first 15 cm are highly liquefied, presenting a clayey texture with slight laminations. Between 19 and 40 cm, we note the presence of polyhedral clay structures. Between 38 and 222 cm, we observed a homogenous clay texture interbedded by seven layers of lacustrine shells (*Melanoides tuberculata*), leading to a visible change in porosity at approximately 62 to 67 cm, 80 cm, 90 cm, 112-114 cm, 124 cm and 140 cm (Fig. S19).

The major element distribution (measured for 5 samples by ICP–MS, Table S1, S2) indicates $Si0_2$ values between 42 and 49% and TiO_2 values between 1.2 and 1.5%. The carbonate content values oscillate between 5 and 10% (Table S1, S2). The plots Si versus Al and Al versus Ca indicate an anticorrelation between terrigenous and carbonated materials; (Fig. S20), suggesting that the carbonate particles mainly originated from the lake and not from the terrigenous fraction supplied by the Awash flood. Similarly, the coefficient for Ca versus Ti is anticorrelated, consequently we will represent the ratio of terrigenous/authigenic sediment components using the Ti/Ca ratio.

The evolution of the Log(Ti/Ca) ratio defines 5 geochemical units (Fig. 5b.1): Unit 1 (0 to 19 cm) is characterized by a gradual increase in Log(Ti/Ca) values. Unit 2 (40 to 19 cm) is characterized by a gradual increase in siliciclastic elements; Unit 3 (115 to 40 cm) presents an abrupt decrease in Log(Ti/Ca) at its base, followed by a progressive increase in Ti; Unit 4 (210 to 115 cm) is characterized by a high lithogenic contribution; Unit 5 (222 to 210 cm) presents a high carbonate content. Between 38 and 222 cm, seven shell beds are characterized geochemically by an increase in Ca and Sr values (Fig. S19).

https://doi.org/10.5194/egusphere-2024-310
Preprint. Discussion started: 5 March 2024

4.3 Chronology

4.3.1 Age model of Lake Afambo sediments

The 173 cm long AFA18-02 sediment was measured using gamma spectrometry to build an age model based on short-lived radionuclides (Fig. 4a.2, 4a.3). The ^{210}Pb excess profile first shows a slow decrease from the top to 105 cm and then a more rapid decrease between 105 and 170 cm until an activity of 26 mBq.g^{-1}. The use of a logarithmic scale to plot these data underscores a poorly constrained (r^2=0.2, related to very high sedimentation rate leading to low activity decreases) single-point alignment that shows a constant sedimentation rate of 108 mm.yr^{-1} for the first 105.8 cm and a better constrained (r^2=0.6) single-point alignment that shows a constant sedimentation rate of 16.5 mm.yr^{-1} between 106 and 170 cm. The change in sedimentation rate occurred in 2009 +/- 7 years. The ^{137}Cs profile shows an increase at the bottom of 4 mBq.g^{-1}. This peak could be associated with the end of maximum nuclear weapon tests in 1963 CE (Foucher et al., 2021; Fig. 4a.3).

Sample ID	Lab ID	Material	Uncalibrated Age		Calibrated ages	
			BP ± yrs (bulk)	F^{14}C ± (%)	2σ cal AD (probability)	Median cal AD
AFA18-02A_10.5-11	SacA57084	Bulk sediment	315 ± 30*			
AFA18-02A_44	SacA57085	Bulk sediment	640± 30*			
AFA18_02A_61	GifA20055/ECHo3328	Fish Bone		1.0456 ± 0.0029	[2008.88 – 2009.58] (30.3%)	2008
AFA18-02A_61	SacA59130	Bulk sediment	610 ± 30*			
AFA18-02A_76	SacA57086	Bulk sediment	365 ± 30*			
AFA18-02B_8-8.5	SacA57087	Bulk sediment	165 ± 30*			
AFA18-02B_35-39	GifA20052/ECHo3259	Vegetal micro remains		1.0940 ± 0.0179	[1993.78 - 2007.1] (90.3%)	2000
AFA18-02B_50.5-51	SacA57088	Bulk sediment	post 1950*			
AFA18-02B_51-53	GifA20053/ECHo3260	Vegetal micro remains		1.1364 ± 0.0123	[1989.86 - 1996.94] (89.3%)	1992
AFA18_02B_66.5	GifA20056/ECHo3327	Fish Bone		1.2069 ± 0.0031	[1984.82 – 1986.45] (52.8%)	1985
AFA18-02B_67	SacA59131	Bulk sediment	320 ± 30*			
AFA18-02B_82.5-83.5	GifA20054/ECHo3261	Vegetal micro remains		1.2357 ± 0.0133	[1980.8 - 1985.76A] (59.9%)	1982
AFA18-02B_81.5-82	SacA57089	Bulk sediment	post 1950*			

***Tab 2**: List of radiocarbon ages on bulk sediment (*), vegetal micro remains and fish bone material. Ages with * are rejected. Calibration curve NH2 (Hua et al., 2013).*

https://doi.org/10.5194/egusphere-2024-310
Preprint. Discussion started: 5 March 2024

Among the 13 samples for ^{14}C ages (Tab. 2), the confrontation with the $^{210}Pb_{ex}$ model shows that the ^{14}C age measured on the bulk sediment organic matter was older, so these ages were systematically rejected (* in Tab. 2). The older ages could be explained by the contamination of reworked micro-organic matter particles from the Awash River catchment. A number of ^{14}C analysis were measured on fish bones and on vegetal micro remains obtained from the micro sampling materials (Fig. S21 and S22). The five ages measured from fish bone and vegetal micro remains are consistent with the ^{210}Pb-derived chronology and are considered viable as part of the age model (Fig. 4a.4). 32 laminae were identified and counted in the F1 and F2 couplets (Fig. 5d), which provides a 106 mm.yr^{-1} sedimentation rate that is highly comparable with the rate derived from the CFCS model (108 mm.yr^{-1}; Fig. 4a.2). Thus, the ^{210}Pb-derived age model confirms that a very high sedimentation rate compatible with the F1 layers could correspond to one season of river-borne discharge.

https://doi.org/10.5194/egusphere-2024-310
Preprint. Discussion started: 5 March 2024

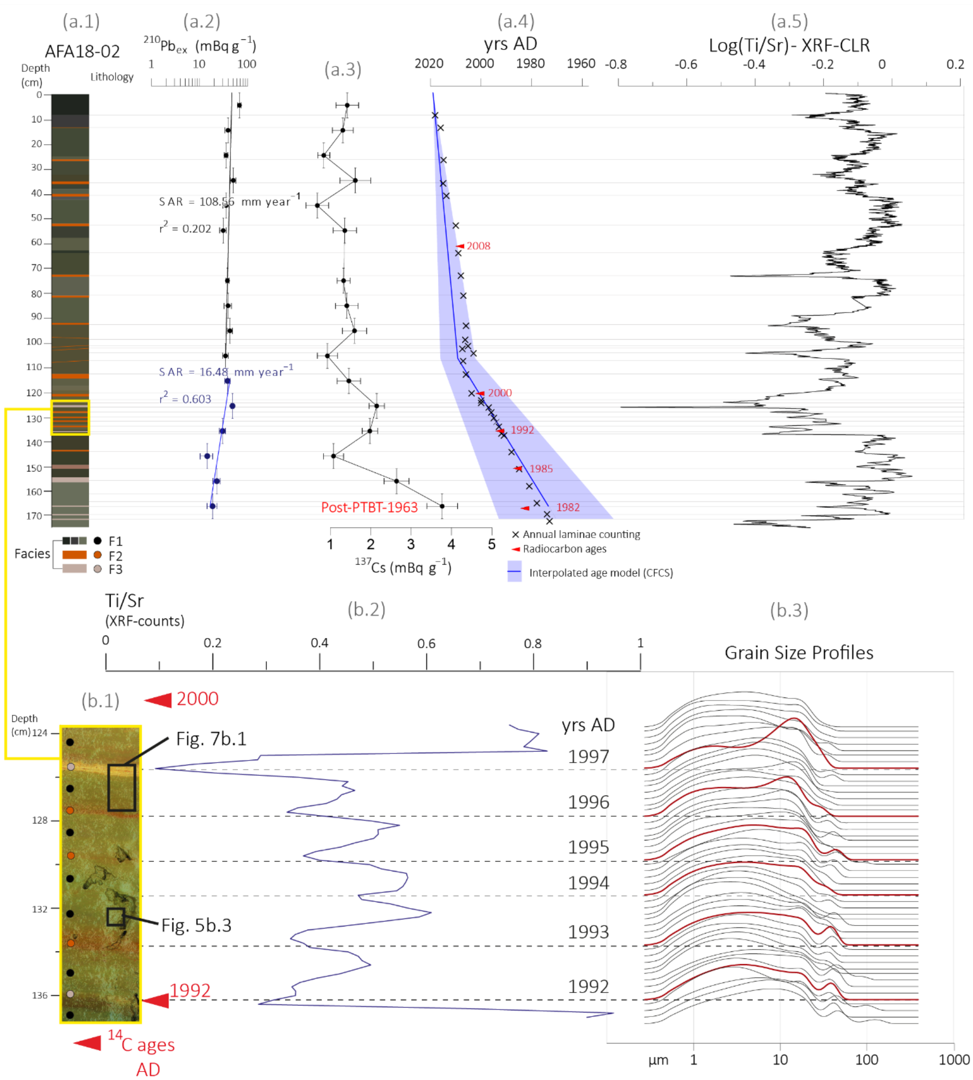

*Figure 4: Age model of the AFA18-02 sequence: **a.1**) lithology; **a.2**) ^{210}Pbex activity profile (mBq.g^{-1}); **a.3**) ^{137}Cs activity profile (mBq.g^{-1}); **a.4**) interpolated CFCS age model with annual laminae counting (crosses) and radiocarbon ages (red arrows); **a.5**) XRF Log(Ti/Sr) ratio transformed with a Centred Log Transformation package (Weltje and Tjallingii, 2008); **b.1**) focus on 124-140 cm F1-F2/F3 couple counting; **b.2**) XRF Ti/Sr (124-140 cm) ratio curve with radiocarbon ages (red) and yrs AD/laminae counting; **b.3**) 124-140 cm grain size profiles (each 2 mm).*

4.3.2 Age model of Lake Gemeri

The upper 66 cm sedimentary sequence of the GEM18-03 core was measured using gamma spectrometry to build an age model based on short-lived radionuclides (Fig. 5a.1, 5a.2). The ^{210}Pb ex profile shows a gradual decrease from 51.8 to 7 mBq.g^{-1}. The use of a logarithmic scale to plot these activities underscores a well-constrained (r^2=0.8) single-point alignment that shows a sedimentation rate of 13.66 mm.yr^{-1} for the first 66 cm (Fig. 5a.2). The ^{137}Cs profile reaches a clear peak between 42 and 48 cm with a maximum activity >10 mBq.g^{-1}. This peak is attributed to the maximum nuclear weapon

https://doi.org/10.5194/egusphere-2024-310
Preprint. Discussion started: 5 March 2024

tests in 1963 CE (Foucher et al., 2021) and is in accordance with the sedimentation rate derived from the ^{210}Pbex profile (Fig. 5a.2). Above this peak, ^{137}Cs activities slowly decrease, which suggests a large catchment area with input of ^{137}Cs already deposited in surface soil and transported by active annual floods (Fig. 5a.3). Among the 13 ^{14}C age samples (Sup. Mat. I), the confrontation with the ^{210}Pb CFCS-derived chronology shows that the ^{14}C ages measured on organic matter are older by several thousands of years, and are therefore rejected with regard to the age model, such as is the case for 8 ages on bulk sediment for the Afambo core age model (Tab. 2). The five ages measured on lacustrine shells (*Melanoides tuberculata*; Murray, 1975) are still older than expected except for the age at 48.5 cm (Fig. S23).

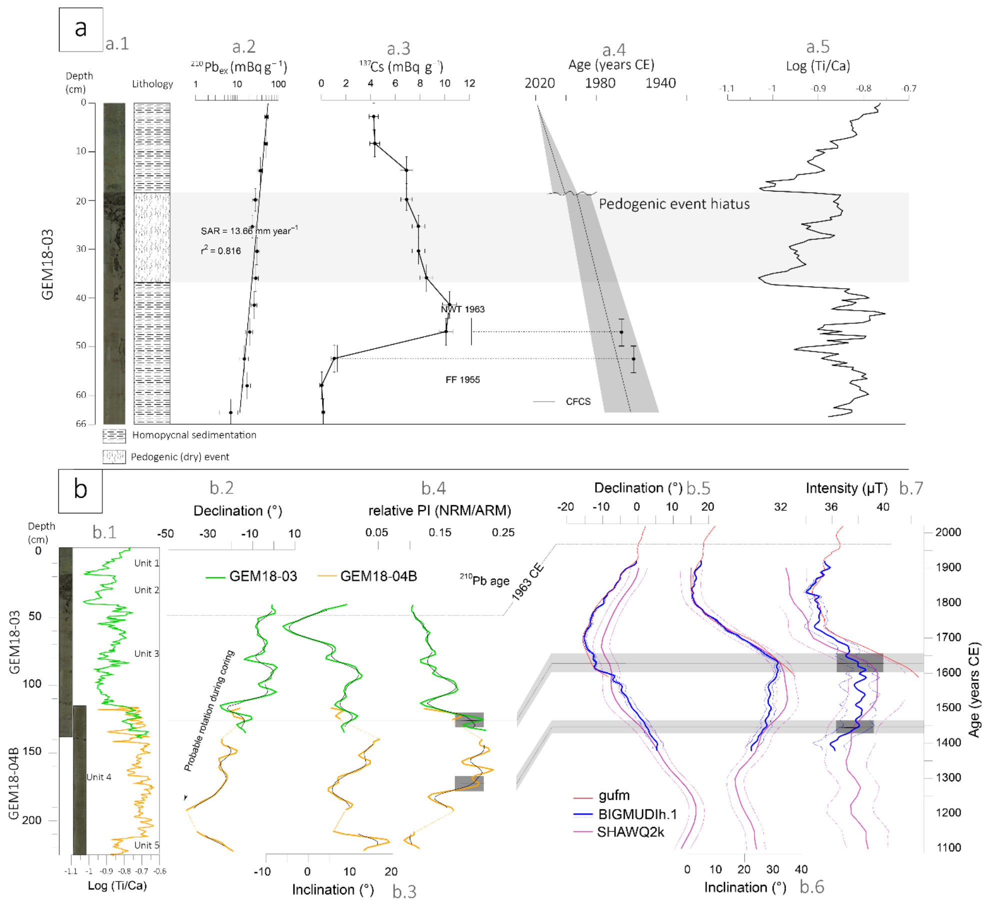

*Figure 5: **a.1**) GEM18-03 upper section (first 66 cm) picture and lithology, **a.2**) ^{210}Pbex and **a.3**) ^{137}Cs profiles, **a.4**) CFCS interpolated age model and **a.5**) Log(Ti/Ca) XRF count intensity. **b.1**) GEM18-03/04B composite section with Log(Ti/Ca) XRF count intensities); correlation between **b.2**) relative palaeo-intensity, **b.2**) inclination and **b.2**) declination measured on GEM18-03/04B with the **b.5 to b.7)** prediction at Lake Gemeri of three geomagnetic global models, BIGMUDIh.1 (in blue, Arneitz et al., 2021), gufm (in red, Jackson et al., 2000) and SHAWQ2k (in purple, Campuzano et al., 2019). BIGMUDIh.1 and SHAWQ2k.1 models are plotted with their 1-σ uncertainty envelope. The correlation is preferentially based on the BIGMUDIh.1 model (see text). For GEM18-03/04B, green and orange thick lines are raw results on GEM18-03 and GEM18-04B sections, respectively, while the thinner black curves show the variation after smoothing with 8-cm sliding windows. The two chronological tie-points are given by RPI, while the secular variation of declination, and to a lesser extent of inclination is likely masked by disturbances during coring.*

https://doi.org/10.5194/egusphere-2024-310
Preprint. Discussion started: 5 March 2024

To better constrain the age model and investigate the sedimentation rate below the first 66 cm dated by short-lived radionuclides, we performed palaeomagnetic measurements with the objective of providing chrono-markers in accordance with the palaeosecular variation in the geomagnetic field over the last millennium (Fig. 5b; Crouzet et al., 2019). The rock magnetic and palaeomagnetic results are detailed in Sup. Mat. D. All rock magnetic results converge towards a homogeneous ferromagnetic mineralogy below 40 cm, composed of almost pure magnetite of relatively fine grain size (pseudo single domain). As the concentration in magnetic grains also does not vary significantly along the core, the magnetic properties are very favourable to the determination of the relative palaeointensity (RPI; Fig. 5b.4). The RPI results with the three possible normalizers (intensity of anhysteretic remnant magnetization ARM, intensity of isothermal remnant magnetization IRM (low-field susceptibility)) are consistent, giving us confidence in our RPI estimation even though it is based on only one core (Fig. 5b). The variations in declination, inclination and RPI below 40 cm are plotted in Figs. 5b.2 and 5b.3. They are compared to the prediction at Lake Gemeri of three geomagnetic global models: gufm (Jackson et al., 2000), SHAWQ2k (Campuzano et al., 2019) and BIGMUDIh.1 (Arneitz et al., 2021; Figs. 5b.5 and 5b.6).
The correlation between the GEM18-03/04B results and the model is not straightforward. However, ^{137}Cs and $^{210}Pb_{ex}$ results from the top of the core allow us to propose a more solid chronological framework of the sedimentary sequence. The almost continuous decrease in declination along the core could suggest that the 190-222 cm depths could correspond to circa 1700 AD. However, the amplitude of the decrease at approximately 40° is much larger than that in the models (approximately 15°), and we strongly suspect that the declination record is biased by a slight progressive rotation feature during coring. Short inclination oscillations in the core are not recognized in the model. Neither the inclination minimum approximately 1840 AD nor the previous fast and regular decrease from 1630 AD are clearly visible in GEM18-03/04B. Higher inclination values are in accordance with the model between 130 and 160 cm.
The period of higher intensity between the middle of the 15th c. and the first half of the 17th c. AD appears to be recorded between 170 cm and 125 cm in GEM18-03/04B. This feature could provide two chrono-markers to establish the age model, 120-130 cm corresponding to 1600-1650 CE and 167-177 cm to 1430-1460 CE. These two proposed tie points are rather consistent with inclination variations because higher values of this parameter are observed in the two ranges of depth and age. The values of correlated depths and ages should be considered approximate regarding the envelope error on the model and because the predictions of global models are generally less reliable in intensity than in declination and inclination (e.g., Brown et al., 2021). Palaeomagnetism measurements based on a single core cannot provide a solid and high-resolution age model. However, the correlation with short-lived radionuclide measurements on GEM18-03 and with the AFA18-02 age model allows us to propose some reliable links with the Awash River hydro-sedimentary chronicles which are at decennial resolution. The palaeomagnetic measurements provide confirmation that ^{14}C ages from GEM18-03/04B are too old, and that these sediments do not exceed the last millennium.

https://doi.org/10.5194/egusphere-2024-310
Preprint. Discussion started: 5 March 2024

4.4 Changes in water surface area at Lakes Gemeri and Afambo, 1985 -

Since 1984, Landsat satellite image data have indicated that Lake Afambo experienced several hydrological fluctuations without a complete drying of the lake. In contrast, Lake Gemeri partially dried up starting in 1984, with a total drying up of the lake between 1990 and 1998 (Fig. 6). Then, between 1999 and 2000, the lake was completely refilled. Comparisons between hydrological, geophysical, sedimentological and geochemical data will be discussed in the next paragraphs.

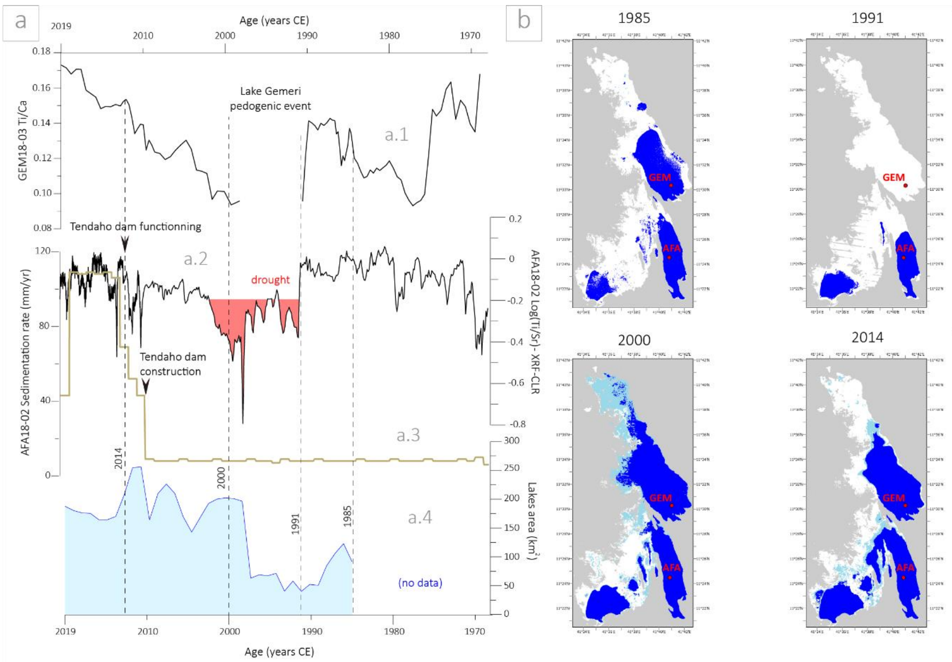

*Figure 6: Hydrosedimentary variability of Lakes Gemeri and Afambo during the last fifty years: **a.1**) Ti/Ca XRF ratio of GEM18-03 sequence; **a.2**) Ti/Ca XRF ratio of AFA18-02 sequence; **a.3**) AFA18-02 sedimentation rate; **a.4**) lake-level area changes since 1985; **b**) map representation of lake area changes in 1895, 1991, 2000 and 2014 CE; white = no water, light blue = 1 month water (temporary water), blue = 12 months of water (permanent water), grey = no data.*

5 - Discussion

5.1- AFA18-02 F1 and F2 significance

5.1.1 – F1 interpretation

In the geological context of the Afar depression and Main Ethiopian Rift (MER), Si, Ti and Ca wt % values of AFA18-02 and GEM18-03/-04B are compared with the same values of 11 mud samples from the Blue Nile headwaters catchment (Bastian et al., 2019) and with 20 basalt samples from the Afar and MER regions (Ayalew et al., 2016), corresponding to the sources of the Awash River catchment (Fig. 7). The Afar lake sediments are well-ranged in SiO_2 wt% values and partially overlap with the TiO_2

https://doi.org/10.5194/egusphere-2024-310
Preprint. Discussion started: 5 March 2024

wt% values of the Ethiopian trap basalts and sediment sources, indicating that the origin of the terrigenous inputs into the lakes is mainly represented by the solid discharge of the Awash River catchment. The ~0.1% offset between the Afar lake sediments and the Ethiopian river sediments and basalts can be attributable to a granulometric sorting effect. Similarly, the lithogenic signature originating from the erosion of stratoid basalt series along the Awash River catchment is confirmed by the ferromagnetic mineralogy of GEM18-03/-04B composed of almost pure magnetite (see section §4.3.2 and Sup. Mat. D).

Thick layers, high organic matter content, coarser grain size (D90 peaks of 25-30 µm, Fig. 9c) dominated terrigenous elements (Si, Ti, Fe, Fig. 7a; EM-1 PCA, Sup. Mat. C) characterize the F1 facies, interpreted as a product of sedimentary load inputs from the Awash River during the wet season, which is associated with the increase in monsoonal precipitation between March and August over the catchment sources located on the Ethiopian Highland (Fig. 1D). The F1 patterns indicate that the total water and solid load inflow during the wet season corresponds to the formation of a particle suspended plume into the lake waters. The lack of erosion features, the disconnection from deltaic geomorphic dynamics and the regular mode of sedimentation (seasonal) indicate that Afambo is a basin characterized by yearly cyclic hydrosedimentary functioning.

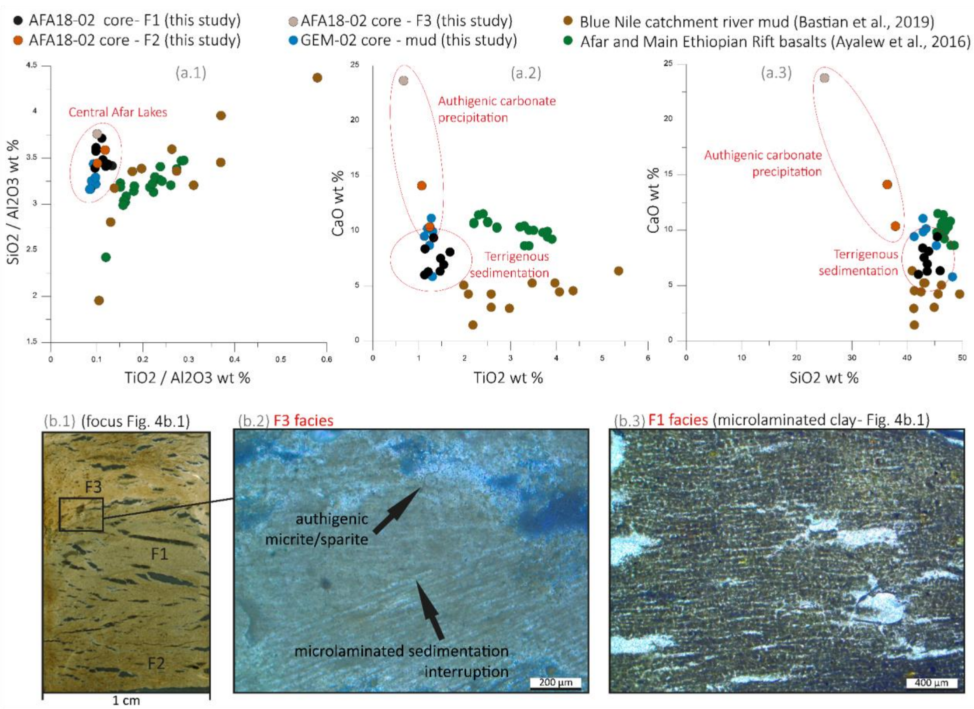

Figure 7: Geochemical and microscopic analyses and interpretation of F1, F2 and F3 facies: ***a.1, 2, 3)*** *SiO2/TiO2, CaO/TiO2 and CaO/SiO2 plots respectively, of Central Afar Lake sediments (black, orange and grey dots; This Study), Blue Nile catchment river muds (green dots; Bastian et al., 2019) and Afar and Main Ethiopian Rift Basalts (brown dots; Ayalew et al., 2016).* ***b.1)*** *Focus scan of this section 125-128 cm depth of AFA18-02 core (XPL);* ***b.2)*** *Microphoto of F3 facies (XPL);* ***b.3)*** *Microphoto of F1 facies (PPL).*

https://doi.org/10.5194/egusphere-2024-310
Preprint. Discussion started: 5 March 2024

5.1.2 – F2 interpretation

The F2 and F3 facies appear to be enriched in CaO of ~5 wt% and ~24 wt%, respectively, and in Sr of ~800 ppm and ~1500 ppm, respectively, as a part of EM-2 of XRF PCA (Sup. Mat. C). Microscopically, such enrichment is observable in the precipitation of sparitic and micritic minerals, showing an interruption of the microlaminated structure typical of F1 (Fig. 7b.2), and suggesting a sedimentation mode and carbonated mineral formation disconnected from the Awash River terrigenous inputs and suspension/sedimentation of fine particles in the lake. Moreover, F2 and F3 are clearly disconnected from the regional mineralogical source cortege (Fig. 7a.2 and 7a.3), indicating how such minerals originate from the lacustrine authigenic activity. Under high evaporation conditions during the dry season, sparitic minerals can be produced directly by chemical or biogenic precipitation into the lake.

Authigenic minerals precipitate when the evaporation rate exceeds the water inflow rate into the lake, leading to a switch from a terrigenous sedimentation pattern to the carbonate mineral precipitation mode. Considering high evaporation rates over the Lake Abhe basin (PE ~2000 mm/yr, Fig. 1E) which are concentrated during the dry season where there is low water inflow, authigenic precipitation of Ca and Sr can represent the direct results of highly saturated waters and the related evaporative processes (Cohen, 2003; Kylander et al., 2011; Martín-Puertas et al., 2011). Indeed, Ca and Sr are related to intra-lake precipitation of $CaCO_3$ with Sr and Ca substitution. This substitution occurs when the chemical concentration of lake waters reaches the point of carbonate saturation, as when lake waters are submitted to a lowering of lake levels (Cohen, 2003). Accordingly, lake surface analyses show that enriched Ca and Sr layers are concomitant with a lowering in Gemeri and Afambo lake levels (Fig. 6a.2). Consequently, F2 and F3 have been interpreted as the occurrence of the dry seasons along the Awash River catchment over the last 50 years, and Ca and Sr elemental values can be used as a marker of drought intensity.

5.2 – Hydro-sedimentary mechanisms between Gemeri and Afambo Lakes

Despite their proximity, Gemeri and Afambo Lakes present divergent patterns of sedimentation, suggesting interdependent and complementary hydro-mechanisms. Located on the prodeltaic front, Lake Gemeri is the first and main receiver of the Awash River waters and sediment, which then overflow into the Afambo basin (Fig. 1). Surprisingly, the ^{210}Pbex activities of both lakes indicate a higher average sedimentation rate in Lake Afambo (~10 $cm.yr^{-1}$) than in Lake Gemeri (~1.36 $cm.yr^{-1}$).

Lake Gemeri is characterized by a shallow water column (average of ~3 m depth measured during the coring and seismic reflection imagery acquisition) in which the extension of the proximal seismic facies into the central part of the basin is observed (Fig. 2). Such evidence suggests how the inputs of the inflow waters create sediment plumes that have expanded in three dimensions from the tributary mouth towards the basin floor. Furthermore, the main homogeneous (non-laminated) structure of the deposits (Fig. 5) suggests the input of continuous turbid currents (no variability in density) from the Awash River

https://doi.org/10.5194/egusphere-2024-310
Preprint. Discussion started: 5 March 2024

waters. Such specific depositional patterns (deposit spatial geometry and sedimentary structure) are attributable to homopycnal-like sedimentation, in which the density of the suspended sediment flow is equal to that of the lake water (Bates, 1953; Chapron et al., 2007). In the absence of water stratification, homopycnal conditions imply the homogeneous mixing of river and lake waters throughout the whole water column by advection processes (Ashley, 2002; Bates, 1953; Chapron et al., 2007). In terms of depositional processes, the occurrence of a homopycnal plume implies a short residence time of water and solid suspended loads in lake waters, leading to reduced sedimentation on the basin floor (Campos et al., 1989) and the development of contrasting sedimentation patterns between proximal and distal basins (Chapron et al., 2007, 2006). Accordingly, most of the solid load transits through Lake Gemeri, producing a low sedimentation rate and erosive facies observed from seismic profiles, which have not been recognized in the distal Lake Afambo basin. Furthermore, the shallow water patterns of Lake Gemeri (~3 m average water-column depth) can promote the re-suspension of the bottom lake sediments after the river floods or during wind-generated waves, reducing the sediment accumulation.

At 17 m water depth (coring site), Lake Afambo sediments show seasonal laminated structures (F1 and F2/3). Facies alternation as well as the microlaminated structure documented in the F1 layers (Fig. 7b.3) indicates the occurrence of rapid decantation processes shortly after each flood, thus suggesting slight water column stratification and a difference between freshwater inputs and lake water density. Particle sedimentation velocities calculated with the Stokes law confirm such observations, providing a mean of ~3 days for the particles to sediment in Afambo lake (Sup. Mat. E). Such sedimentary patterns combined with the absence of erosive or turbiditic events suggest a hypopycnal character of the inflow waters/solid load into Afambo Lake. Hypopycnal plume formation at the tributary mouth of Lake Afambo can be made possible by the decrease in the current energy flow and by the loss of density of the waterfront by the trapping of fine sediments into the deltaic marshes occurring between the two lakes (Fig. 1). Accordingly, the <3.9 µm fraction is represented by 60-80% in Lake Gemeri and by 20-35% in Lake Afambo (Sup. Mat. J). Other factors that could influence the formation of hypopycnal plumes in Afambo Lake are the reduced energy flow into the lake waters due to the endorheic patterns of the basin (no outflow towards Lake Abhe) and a larger water-column depth.

The explanation of the general hydro-sedimentary modes of functioning of the two basins indicates **a**) a first prodeltaic basin (Gemeri) with lower sedimentation rates, dominated clayey texture, erosive processes and deltaic dynamics-dependant, which have recorded the general trends (decennial) of hydrological fluctuations of the Awash catchment over a long period (~700 yrs) in our study; **b**) a second distal basin (Afambo) with higher sedimentation rates, clayey texture and seasonal F1 and F2/3 deposits, which records in high-resolution (interannual) the hydrological fluctuations of the Awash River catchment during a short period (~50 yrs).

https://doi.org/10.5194/egusphere-2024-310
Preprint. Discussion started: 5 March 2024

5.3– Multi-centennial hydro-sedimentary trends from Lake Gemeri sediments

Similar to AFA18-02, PCA on XRF data of the Gemeri sequence (Fig. S6) show three main geochemical end-members: the terrigenous one composed of Ti, SI, Al, K, Zr, Fe, Mn, and Mg; the evaporitic (Ca and Sr); and the organic component (S and Br). Diachronic variations in these main components along the GEM18-03/-04 core allow us to define two kind of periods: "Humid pluriannual periods" are characterized by high terrigenous content such as Ti from high water flow activity of the Awash River. Contrastingly, "dryer pluriannual periods" are characterized by the enrichment of Ca and Sr element values interpreted as evaporative processes as a result of higher evaporation and reduced water inflow into the lakes (Fig. 8). Thanks to the composite short-lived radionuclides and palaeomagnetism age model on the GEM18-03/04 sequence (Fig. 5b), we are able to discuss the general hydrological trends (centennial resolution) for the period ranging between 1300 and 1964 CE.

Between 1300 and 1650 CE, relatively high and constant Ti/Ca ratio values were recorded (Fig. 5b.1). This indicates how this period is characterized by high detrital inputs into the Lake Abhe basin, likely induced by water inflow processes over the Awash River basin. Following a drop in Ti proxy between 1650 and 1750 CE, the catchment could have experienced a gradual increase in water and solid load flow until 1979 CE, as deduced from the increase in Fe, Ti and Si elemental content. The last decade (1968-1979 CE) is thus characterized by higher supplies compared to the following periods. Geomorphologically, during this time, the Awash palaeo-delta was likely characterized by an anastomosing river network pattern that fed the prodeltaic lakes and marshes from the southwest to the northeast of the alluvial plain (Fig. 8a).

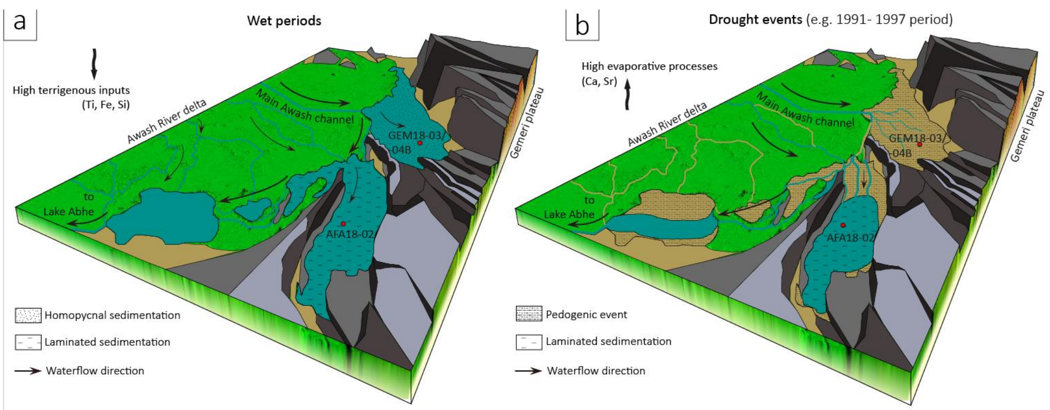

*Figure 8: Schematic interpretative model of hydro-sedimentary patterns of the Awash River delta (including lakes Gemeri and Afambo) during enhanced wet periods (**a**) and drought events (**b**).*

https://doi.org/10.5194/egusphere-2024-310
Preprint. Discussion started: 5 March 2024

5.4 - ~50-year-long seasonal drought and flood chronicle from Lake Afambo

In the AFA18-02 core, F1 and F2/F3 layers are interpreted as a result of the sedimentary interannual response of Central Afar Lake basins to wet and dry seasonal discharge of the Awash River. Thanks to the multi-proxy geochronological approach, we are able to propose a solid age model covering the period between 1969 AD and 2019 AD. The aim of this section is to provide a wet and dry season magnitude chornicle for the last ~50 years across the Awash River basin through **a**) the estimation of the wet season inflow intensity recognized in F1 layers and **b**) the estimation of drought/evaporitic process intensities recognized in dry season F2/F3 layers (see section §5.1 for the facies interpretation).
With the aim of reconstructing the intensity of the Awash River wet season intensities, we selected two proxies: the grain size and the thickness of the F1 layers. Thanks to well-established published data, we are able to propose an interpretation of the river energy discharge based on the grain-size data (e.g., Campbell, 1998; Lapointe et al., 2012; Parris et al., 2010; Sabatier et al., 2022, 2017; Wilhelm et al., 2015). Indeed, the coarse grain size fraction (Q90) has been successfully used to track hydrologic conditions, particularly the transport capacity and the stream velocity during flood events, such as the intensity of past floods (Gilli et al., 2013; Molinaroli et al., 2009; Parris et al., 2010). Similarly, previous studies interpret the thickness of flood deposits in lakes as the total volume of solid material transported and deposited during flood events (Jenny et al., 2014; Schiefer et al., 2011; Wilhelm et al., 2015, 2012). Assuming that the F1 layers are not the result of a unique flood event but the sum of flood events that occurred during the wet season, we can consider the F1 layer thickness and Q90 as proxies of the Awash discharge intensity in terms of flow energy and the volume of solid load that occurred during the wet monsoonal period between March and August. In our case, the striking similitudes between D90 peaks and thickness of F1 layers (Fig. 9b, c) confirms the combination of proxies for tracking the flood intensities.
To reconstruct the intensity of the dry season, we use Sr and Ca elements (Fig. 3) and the Ti/Sr elemental ratio (Fig. 9) as a marker of evaporative processes resulting from reduced water flow inputs, the contraction of the lake surface and high temperatures as explained in detail in section §5.1.2. The relationship between enhanced carbonate precipitation and drought intensity in Lake Afambo is evident in the F3 layer at 126 cm, corresponding to the 1997 CE dry season (Fig. 4), in which the highest Ca and Sr values recorded in the core correspond to the lowest lake level ever observed (Fig. 6) and the strongest impact of El Niño that has ever been historically recorded over East Africa (Fig. 9; Palmer et al., 2023).
The comparison between Ti/Sr, F1 thickness and D90 proxies (Fig. 9a, b and c) shows a strong relationship between physicochemical authigenic processes (carbonate precipitation and Sr enrichment linked to evaporative trends in the dry season) and the Awash River solid load inputs into the lake (linked to the increase or the reduction of water flow at the yearly scale). Consequently, we are able to discuss

https://doi.org/10.5194/egusphere-2024-310
Preprint. Discussion started: 5 March 2024

the variability of the wet seasons and drought intensities in the Central Afar region over the last ~50 years.

Between 1969 and 1979, a gradual increase in both F1 thickness and D90 indicates a decennial intensification of wet season solid/liquid Awash river discharge, with two years of demarcated wet season floods in 1976 and 1978. Decrease of Ti/Sr indicate an enhanced dry season in 1969, 1978 and 1979. Between 1980 and 1990, a general and constant trend of high river discharge was recorded with enhanced floods in the 1981, 1982, 1988 and 1989 wet seasons. A pronounced drought was recorded in 1983/1984.

From 1991 to 1997, the occurrence of an abrupt lowering thickness of F1 and low and constant D90 indicate reduced river load inputs compared to the previous and following periods, suggesting a reduced river discharge intensity during the wet season. Such weak river discharge is in accordance with the lowest level recorded for Lake Afambo, the drying of Gemeri Lake (Fig. 6a.4) and high evaporative processes of lake waters (Sr peaks), especially between 1991 and 1997, highlighting the occurrence of the most severe drought period that has been recorded over the last ~50 years in the Central Afar Region.

Between 1998 and 2010, constant Ti/Sr and increase of F1 thickness proxies indicate a gradual increase in river terrigenous inputs in relation to weak dry season drought intensities, except for two years of dry season droughts recorded in 2009 and 2010. The high variable D90 suggests the alternation between yearly high- and low-energy inflow, highlighting a year-by-year hydrological instability of the Awash River catchment for this period.

Since the 2010 wet season, the AFA18-02 sequence records a disproportionate increase in sedimentation rate (Fig. 6a.3) and in yearly solid load volume inputs (F1 thickness Fig. 9b), in concomitance with a reduced river energy discharge (low and constant D90) and an average lake water surface decrease of ~100 km^2 compared to the previous decade (Fig. 6). Such a hydro-sedimentary anomaly could be attributable to a strong anthropogenic impact such as that induced by the construction of the Tendaho Dam and the related Tendaho reservoir (Dereje et al., 2018; Yemane, 2008). Indeed, between 2010 and 2014, the dam project included the reorganization of the hydrographic network of the Lower Awash plain with the massive development of irrigation channels, sugarcane cultivation and a sugar factory (corresponding to the alluvial plain area in Fig. 1B). The increase in solid load discharge could thus be linked to the disproportionate intensification of local soil erosion induced by artificial channel digging and agricultural exploitation of the lower Awash plain. Accordingly, the reduced river flow energy and lake surfaces are related to the water retention of the artificial Tendaho reservoir at the mouth of the Lower Awash plain. For this period, our geochemical and sedimentological data are not discussed in terms of regional climate-induced drought and flood intensities because they are partially disconnected from the regional hydrological dynamics of the Awash River catchment.

https://doi.org/10.5194/egusphere-2024-310
Preprint. Discussion started: 5 March 2024

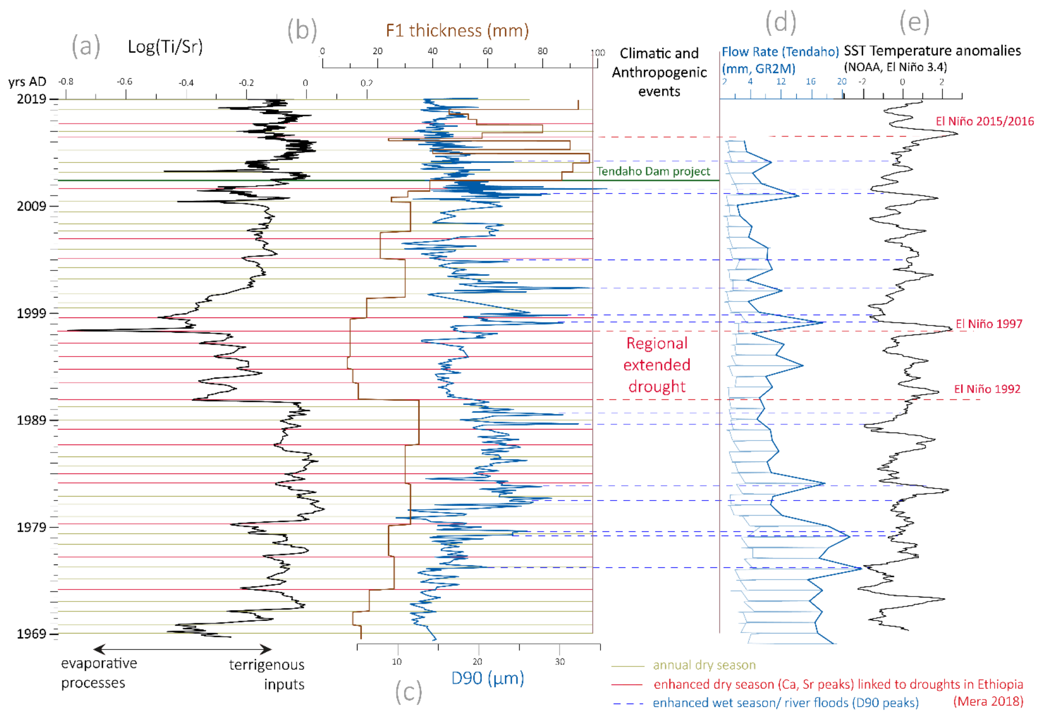

***Figure 9**: Fifty years of Awash seasonal flood/drought magnitudes and their connection with ENSO events recorded in the AFA18-02 sequence: **a)** Log(Ti/Sr) XRF ratio; **b)** F1 thickness; **c)** D90; **d)** water flow rate at Tendaho (mm, GR2M); **e)** SST temperature anomalies (NOAA, El Niño 3.4) with indicated annual F2 laminae (dry season, yellow lines), enhanced dry interannual events (red lines) and enhanced wet season/river flood periods (blue lines).*

5.3 Magnitudes of the Awash River wet/drought seasons, and their connection with the impacts of ENSO events

Between March and August across Eastern Africa, the monsoonal rainy season is vital for agricultural production and thus for national food security, especially in more susceptible areas such as along the Rift Valley and over distal lowlands. During the last ~50 years, recurrent anomalous low and reduced rainy seasons have had substantial environmental, humanitarian and economic impacts, including agriculture and ecosystem sustainability (Palmer et al., 2023). Recent studies have highlighted how the post-1960s period is characterized by global enhanced ENSO SST variability and magnitude related to anthropogenic activities (rising CO_2 atmospheric concentrations and decreased sulfur aerosols; Cai et al., 2023; Grothe et al., 2020). Post-1960 periods are thus marked by global increased variability features evident in more frequent occurrences of strong El Niño and strong La Niña events (Cai et al., 2023). In Ethiopia, the coincidence of enhanced ENSO episodes and droughts was recorded in 1965, 1972–73, 1982–83, 1986, 1991–93, 1997–98 and 2015-16 (Comenetz and Caviedes, 2002; Mera, 2018). In the Horn of Africa, rainfall anomalies of ~100–250 mm $year^{-1}$ were documented in 1997, 2006, 2012, 2015 and 2019 and are associated with ENSO and IOD variability and socioeconomic crises (Nicholson,

https://doi.org/10.5194/egusphere-2024-310
Preprint. Discussion started: 5 March 2024

2017; Palmer et al., 2023; Spencer et al., 2005; Webster et al., 1999). Today (until December 2023), ~22 million people are expected to confront acute food insecurity similar to the El-Nino-induced drought-affected areas of Djibouti, Ethiopia, Kenya and Somalia, and will face what is estimated to be the worst drought of the last 40 years (FAO, 2023, 2022).

Together with reduced anomalous precipitation during long rainy seasons, subsequent disproportionate short flood events were often recorded, and affected crop production as well as increasing the number of tropical disease outbreaks. For example, during the 1958/59 El Niño event, abnormally high temperature, floods, and relative humidity resulted in 3 million malaria cases across the Ethiopian highlands (Fontaine et al., 1961). During the El Niño of 1997-1998, exceptionally short heavy rains and floods affected food production and distribution networks throughout Eastern Africa. The floods caused extensive damage to crops, losses of large numbers of livestock and an increased incidence of cholera, malaria and rift valley fever linked to the lack of potable water in flooded areas (Palmer et al., 2023). The repetition of such events continues today as recorded in 2022, during which the meagre rainy season was followed by prolonged floods (OCHA, 2022).

In order to expand our knowledge base and mitigate difficulties with regards to future adaptation to such extreme changes, it is pivotal to fully understand not only Eastern African seasonal rainfall dynamics, but also regional to local hydraulic system feedbacks to ENSO flood and drought events.

East African atmospheric climate modes may operate concurrently between the Indian Ocean Dipole (IOD), South Atlantic SST and ENSO, making it difficult to understand the origin, magnitude and temporal variability of extreme droughts or flooding events (Emerton et al., 2017; Ficchì et al., 2021). Generally, the link between ENSO and IOD anomalies appears to be underestimated in model predictions for East African rainfall during strong El Niño periods (MacLeod and Caminade, 2019). Recent simulation studies have shown that it is difficult to estimate ENSO-induced flood and drought hazards in Sub-Saharan Africa as there are significant regional differences which are not sufficiently studied. Indeed, the Main Ethiopian Rift and the Awash River catchment areas are underrepresented in ENSO and IOD climate teleconnection models (Ficchì et al., 2021), reinforcing the importance of our data in the framework of current climatic anomaly studies.

The comparison between our wet/dry season intensity reconstruction, the flow rate modelling of the Awash River at Tendaho Lake, and the SST anomalies of the NOAA El Niño model allow us to discuss the high-resolution seasonal hydro-climate variability of the Awash River catchment in relation to El Niño atmospheric anomalies (Fig. 9).

We have observed a generally stronger drought in our record during El Niño years, which are known to be associated with low discharge, while La Niña years correspond with relatively high discharge (Abtew et al., 2009; Amarasekera et al., 1997; Camberlin et al., 2001; De Putter et al., 1998; Eltahir, 1996; Wang and Eltahir, 1999; Zaroug et al., 2014; Fig. 9). We have also observed that the occurrence of extreme wet season conditions at the onset of La Niña periods seems proportional to the gradient amplitude between positive and negative ENSO SST temperature anomalies, as is evident in 1998 (Fig. 9).

https://doi.org/10.5194/egusphere-2024-310
Preprint. Discussion started: 5 March 2024

Accordingly, the D90 variability of the AFA18-02 core indicates the occurrence of high hydrological activity during 1975, 1978, 1981/82, 1988/89 years following El Niño-induced droughts documented in 1975/76, 1978/79, 1982 and 1987/88 in Ethiopia (Mera, 2018). Overall, along the Afambo sequence, all major El Niño-induced droughts are systematically well recorded by our proxy of drought intensity (red lines Fig. 9; Mera, 2018).

High evaporation processes and low fluvial solid load inputs recorded in the AFA18-02 sequence suggest that along the Lower Awash valley, the period between 1991 and 1997 experienced the most extreme and continuous drought in the region of the last ~50 years (Fig. 9). In the Lake Abhe basin, such an event caused the complete drying of Lake Gemeri and a substantial lowering of Lake Afambo (Fig. 6b), suggesting loss of water capacity of the lower Awash plain agricultural fields. In East Africa, the 1997/1998 El Niño tended to have significant socio-economic and health impacts on populations even if it was not as extreme or as widespread as that of 1984 (Palmer et al., 2023). In contrast, the sedimentary record of the Afar lakes has revealed that the 1997 drought was more intense than the 1984 drought. Such discrepancy can be attributable to strong regional variability, with particularly arid areas such as the Afar region being more impacted by drought than other East African regions. Accordingly, *United Nations Emergencies Unit for Ethiopia* reports highlight how the 1997 drought was particularly virulent in the Somali Regional state and the Afar, located in the southeast of the Horn of Africa (Borton, 1997). As a result of low rains in 1996 and 1997, more than 275,000 people in the Afar Regional State were reported to be affected by drought.

At the scale of the Horn of Africa, 1997 is considered to have had socioeconomic impacts principally related to the La Niña flooding events. From October to December 1997, exceptionally heavy rains seriously affected food production throughout Eastern Africa (CARE, 1998; Nicholson, 2017). Accordingly, immediately after the extreme drought of the 1997 dry season, we observe a disproportionate increase in Awash River solid load inputs that were concomitant with La Niña (Fig. 9).

From April 2016 to December 2017, the southeastern regions of the Horn of Africa experienced the strongest drought of the last ~40 years which have been linked to the El Niño 2015 event (MacLeod and Caminade, 2019; Mera, 2018). Even if modulated by the Tendaho dam, we observe three consecutive years of reduced sedimentation rates and unwanted evaporation processes from the Afambo sequence indicating that the lower Awash valley had been impacted by anomalously weak rainy seasons in 2015 and 2016. In the nearby Somali region, such events triggered acute food shortages and malnutrition exacerbated by a shortage of potable water that led to disease outbreaks, which affected more than six million people (FSNAU, 2022; WBG, 2018).

The AFA18-02 sequence has been shown to be an exceptional record of anomalous hydrological events in the region, but quantitative data for regional to local climate change impacts are still lacking. Indeed, our record provides high-resolution wet season and drought magnitude records, highlighting some similarities and divergences compared to historical and instrumental records, which are necessary for the improvement of Eastern African climate prediction models. This data merits integration into models

https://doi.org/10.5194/egusphere-2024-310
Preprint. Discussion started: 5 March 2024

to test different external forcings and large-scale climate teleconnections and feedbacks (vegetation, dust concentration, IOD, South Atlantic SST, relationship between ENSO and summer monsoon variability), which have affected inter-annual to multi-centennial hydrological variability in East Africa.

6 Conclusion

In this study, we have demonstrated that the hydro-sedimentary patterns of Central Afar Lakes (Ethiopia) are highly sensitive to changes in yearly precipitation over the Awash River catchment. Using a solid age model, sedimentological and geochemical proxies and microscopic observation on two lacustrine cores cross-referenced with a lake surface reconstruction model from satellite images and seismic imagery, we provide a high-resolution seasonal record of Awash River wet seasons/droughts covering the last ~50 years . Atmospheric anomalies linked to ENSO SST variability are the main factors determining hydrological instability over the Central Afar basin during the last fifty years in terms of flood hazards and drought periods. Between 1969 and 1989, our record shows increased wet season flood activity of the Awash River linked to La Niña, with a moderate impact of the 1984 El Niño on evaporative conditions in the Lake Abhe basin. Between 1991 and 1997, we highlight the occurrence of the strongest prolonged drought ever recorded in the Central Afar Lake region, and demonstrate similarities and divergences between our data and instrumental and historical drought records. This study provides new unpublished data on the impact of ENSO in the region and confirms the utility of this unique quantitative record for the improvement of future regional climate predictions. From a local perspective, we provide robust evidence to demonstrate how the construction of the Tendaho dam along the Awash River associated with extensive agricultural management, strongly affected the hydrosedimentary balance of the Lower Awash Valley from 2010, likely resulting in a disproportionate increase in local soil erodibility along the alluvial plain.

The reactivity of local to regional hydrology and soil to global changes remains understated in East African climatic models. This paper demonstrates the importance of studies on regional hydro-system feedbacks to global atmospheric anomalies, to better understand and mitigate the sometimes catastrophic effects of global warming in extreme environments such as the Afar, especially in the context of current climate-induced food insecurity in East Africa (2022-2023 season) and dire predictions for what is ahead.

Code and Data availability

The detailed core location and coring information are available on the Cyber Carothèque Nationale of CNRS (https://cybercarotheque.fr/). All analytical data presented in this manuscript are available in the Supplementary Material document.

https://doi.org/10.5194/egusphere-2024-310
Preprint. Discussion started: 5 March 2024

Author contribution

C. Mologni: Conceptualization, Data curation, Formal analysis, Investigation, Supervision, Validation, Visualization, Writing – original draft preparation - review and editing.

M. Revel: Conceptualization, Funding acquisition, Investigation, Project administration, Supervision, Writing – original draft preparation– review & editing.

E. Chaumillon: Conceptualization, Investigation, Formal analysis, Data curation, Visualization, Writing– original draft preparation – review & editing.

E. Malet: Formal analysis, Investigation, Methodology, Resources.

T. Coulombier: Formal analysis, Investigation, Methodology, Resources.

P. Sabatier: Conceptualization, Data curation, Formal analysis, Investigation, Resources, Visualization, Writing– original draft preparation – review & editing.

P. Brigode: Conceptualization, Data curation, Formal analysis, Investigation, Writing– original draft preparation – review & editing.

G. Hervé: Conceptualization, Data curation, Formal analysis, Investigation, Visualization, Writing – original draft preparation – review & editing.

A.-L. Develle: Data curation, Formal analysis, Investigation, Methodology, Resources.

L. Schenini: Data curation, Formal analysis, Investigation.

M. Messous: Data curation, Formal analysis, Investigation, Methodology, Resources.

G. Davtian: Data curation, Formal analysis, Investigation, Methodology, Resources.

A. Carré: Formal analysis, Investigation, Methodology, Resources.

D. Bosch: Formal analysis, Methodology, Resources.

N. Volto: Conceptualization, Data curation, Formal analysis, Investigation, Writing – original draft preparation – review & editing.

C. Méndard: Project administration, Resources.

L. Khalidi: Conceptualization, Funding acquisition, Project administration, Supervision, Writing - review & editing.

F. Arnaud: Conceptualization, Investigation, Project administration, Data curation, Supervision, Ressources, Writing – original draft preparation– revie

Competing Interests

The authors declare that they have no conflict of interest

Acknowledgements

The CLIMAFAR (PIs: L. Khalidi & M. Revel) December 2018 coring operations were carried out in the framework of the VAPOR-Afar project (PI: L. Khalidi) with a permit granted by the

https://doi.org/10.5194/egusphere-2024-310
Preprint. Discussion started: 5 March 2024

Ethiopian Authority for Research and Conservation of Cultural Heritage (ARCCH, Addis Ababa, Ethiopia) in collaboration with the Afar Bureau of Tourism & Culture. Funding for CLIMAFAR was granted by the French government, and managed by the Agence Nationale de la Recherche under the Investissements d'Avenir UCAJEDI project, reference no. ANR-15-IDEX-01 . XRF-Core Scanner and thin section fabrication were performed at the EDYTEM laboratory with funding from the CLIMAFAR grant. XRD analyses were funded by a University Cote d'Azur doctoral grant (C. Mologni). Radiocarbon dating was performed with funding from an ARTEMIS grant and support from the Geoazur laboratory (M. Revel) using the MIChadas facilities (Christine Hatté; LSCE – UMR 8212 CEA-CNRS-UVSQ). The authors thank the Laboratoire Souterrain de Modane (LSM) facilities for the gamma spectrometry measurements and Environnement, Dynamique et Territoires de Montagne (EDyTeM) for the X-ray fluorescence analyses (A.-L. Develle). We would like to thank the Ethiopian ARCCH, the Afar Bureau of Tourism & Culture and the French Center for Ethiopian Studies (CFEE) for their authorization and support with regards to fieldwork and logistics. We also thank Dr. Tatiana Theodoropoulou and Dr. Lucie Coudert for the fish species determination of the AFA18-02 core sequence.

References

Abtew, W., Melesse, A.M., Dessalegne, T., 2009. El Niño Southern Oscillation link to the Blue Nile River Basin hydrology. Hydrological Processes 23, 3653–3660. https://doi.org/10.1002/hyp.7367

Amarasekera, K.N., Lee, R.F., Williams, E.R., Eltahir, E.A.B., 1997. ENSO and the natural variability in the flow of tropical rivers. Journal of Hydrology 200, 24–39. https://doi.org/10.1016/S0022-1694(96)03340-9

Arnaud, F., Poulenard, J., Giguet-Covex, C., Wilhelm, B., Révillon, S., Jenny, J.-P., Revel, M., Enters, D., Bajard, M., Fouinat, L., Doyen, E., Simonneau, A., Pignol, C., Chapron, E., Vannière, B., Sabatier, P., 2016. Erosion under climate and human pressures: An alpine lake sediment perspective. Quaternary Science Reviews 152, 1–18. https://doi.org/10.1016/j.quascirev.2016.09.018

Arnaud, F., Sabatier, P., 2022. Lakes as Recorders of Earth Surface Dynamics From Yearly to Plurimillennial Time-Scales, in: Mehner, T., Tockner, K. (Eds.), Encyclopedia of Inland Waters (Second Edition). Elsevier, Oxford, pp. 439–452. https://doi.org/10.1016/B978-0-12-819166-8.00125-0

Arneitz, P., Leonhardt, R., Egli, R., Fabian, K., 2021. Dipole and Nondipole Evolution of the Historical Geomagnetic Field From Instrumental, Archeomagnetic, and Volcanic Data. Journal of Geophysical Research: Solid Earth 126, e2021JB022565. https://doi.org/10.1029/2021JB022565

Ashley, G.M., 2002. 11 - Glaciolacustrine environments, in: Menzies, J. (Ed.), Modern and Past Glacial Environments. Butterworth-Heinemann, Oxford, pp. 335–359. https://doi.org/10.1016/B978-075064226-2/50014-3

https://doi.org/10.5194/egusphere-2024-310
Preprint. Discussion started: 5 March 2024

Ayalew, D., Jung, S., Romer, R.L., Kersten, F., Pfänder, J.A., Garbe-Schönberg, D., 2016. Petrogenesis and origin of modern Ethiopian rift basalts: Constraints from isotope and trace element geochemistry. Lithos 258–259, 1–14. https://doi.org/10.1016/j.lithos.2016.04.001

Bajard, M., Poulenard, J., Sabatier, P., Develle, A.-L., Giguet-Covex, C., Jacob, J., Crouzet, C., David, F., Pignol, C., Arnaud, F., 2017. Progressive and regressive soil evolution phases in the Anthropocene. CATENA 150, 39–52. https://doi.org/10.1016/j.catena.2016.11.001

Bajard, M., Sabatier, P., David, F., Develle, A.-L., Reyss, J.-L., Fanget, B., Malet, E., Arnaud, D., Augustin, L., Crouzet, C., Poulenard, J., Arnaud, F., 2016. Erosion record in Lake La Thuile sediments (Prealps, France): Evidence of montane landscape dynamics throughout the Holocene. The Holocene 26, 350–364. https://doi.org/10.1177/0959683615609750

Barberi, F., Varet, J., 1977. Volcanism of Afar: Small-scale plate tectonics implications. Geol. Soc. Am. Bull., 88, 1251–1266.

Bastian, L., Vigier, N., Revel, M., Yirgu, G., Ayalew, D., Pik, R., 2019. Chemical erosion rates in the upper Blue Nile Basin and related atmospheric CO2 consumption. Chemical Geology 518, 19–31. https://doi.org/10.1016/j.chemgeo.2019.03.033

Bates, C.C., 1953. RATIONAL THEORY OF DELTA FORMATION1. AAPG Bulletin 37, 2119–2162. https://doi.org/10.1306/5CEADD76-16BB-11D7-8645000102C1865D

Beck, H.E., Wood, E.F., Pan, M., Fisher, C.K., Miralles, D.G., Dijk, A.I.J.M. van, McVicar, T.R., Adler, R.F., 2019. MSWEP V2 Global 3-Hourly 0.1° Precipitation: Methodology and Quantitative Assessment. Bulletin of the American Meteorological Society 100, 473–500. https://doi.org/10.1175/BAMS-D-17-0138.1

Bertin, X., Chaumillon, E., 2005. New Insights in Shallow Gas Generation from Very High Resolution Seismic and Bathymetric Surveys in the Marennes-Oléron Bay, France. Mar Geophys Res 26, 225–233. https://doi.org/10.1007/s11001-005-3720-y

Borton, J., 1997. Ethiopia Monthly Information Report Apr 1997. United Nations Emergencies Unit for Ethiopia (UN-EUE).

Borton, J., 7. Ethiopia Monthly Information Report March 1997. United Nations Emergencies Unit for Ethiopia.

Brown, M.C., Hervé, G., Korte, M., Genevey, A., 2021. Global archaeomagnetic data: The state of the art and future challenges. Physics of the Earth and Planetary Interiors 318, 106766. https://doi.org/10.1016/j.pepi.2021.106766

Bruel, R., Sabatier, P., 2020. serac: an R package for ShortlivEd RAdionuclide chronology of recent sediment cores. Journal of Environmental Radioactivity 225, 106449. https://doi.org/10.1016/j.jenvrad.2020.106449

Cai, W., Ng, B., Geng, T., Jia, F., Wu, L., Wang, G., Liu, Yu, Gan, B., Yang, K., Santoso, A., Lin, X., Li, Z., Liu, Yi, Yang, Y., Jin, F.-F., Collins, M., McPhaden, M.J., 2023. Anthropogenic impacts on twentieth-century ENSO variability changes. Nat Rev Earth Environ 1–12. https://doi.org/10.1038/s43017-023-00427-8

Camberlin, P., Janicot, S., Poccard, I., 2001. Seasonality and atmospheric dynamics of the teleconnection between African rainfall and tropical sea-surface temperature: Atlantic vs. ENSO. International Journal of Climatology 21, 973–1005. https://doi.org/10.1002/joc.673

Campbell, C., 1998. Late Holocene Lake Sedimentology and Climate Change in Southern Alberta, Canada. Quaternary Research 49, 96–101. https://doi.org/10.1006/qres.1997.1946

Campos, H., Steffen, W., Aguero, G., Parra, O., Zuniga, L., 1989. Estudios limnológicos en el Lago Puyehue (Chile) : morfometria, factores fisicos y quimicos, plancton y productividad primaria. Medio ambiente (Valdivia) 10, 36–53.

Campuzano, S.A., Gómez-Paccard, M., Pavón-Carrasco, F.J., Osete, M.L., 2019. Emergence and evolution of the South Atlantic Anomaly revealed by the new paleomagnetic reconstruction SHAWQ2k. Earth and Planetary Science Letters 512, 17–26. https://doi.org/10.1016/j.epsl.2019.01.050

CARE, 1998. El Niño in 1997-1998: Impacts and CARE's Response.

Chapron, E., Ariztegui, D., Mulsow, S., Villarosa, G., Pino, M., Outes, V., Juvignié, E., Crivelli, E., 2006. Impact of the 1960 major subduction earthquake in Northern Patagonia (Chile, Argentina). Quaternary International, Holocene environmental catastrophes in South America: from the lowlands to the Andes 158, 58–71. https://doi.org/10.1016/j.quaint.2006.05.017

Chapron, E., Juvigné, E., Mulsow, S., Ariztegui, D., Magand, O., Bertrand, S., Pino, M., Chapron, O., 2007. Recent clastic sedimentation processes in Lake Puyehue (Chilean Lake District, 40.5°S). Sedimentary Geology 201, 365–385. https://doi.org/10.1016/j.sedgeo.2007.07.006

Cohen, A.S., 2003. Paleolimnology: The History and Evolution of Lake Systems. Oxford University Press.

Comenetz, J., Caviedes, C., 2002. Climate variability, political crises, and historical population displacements in Ethiopia. Global Environmental Change Part B: Environmental Hazards 4, 113–127. https://doi.org/10.1016/j.hazards.2003.08.001

Coron, L., Delaigue, O., Thirel, G., Dorchies, D., Perrin, C., Michel, C., 2022. airGR: Suite of GR Hydrological Models for Precipitation-Runoff Modelling (v. 1.7.0). airGR.

Coron, L., Thirel, G., Delaigue, O., Perrin, C., Andréassian, V., 2017. The suite of lumped GR hydrological models in an R package. Environmental Modelling & Software 94, 166–171. https://doi.org/10.1016/j.envsoft.2017.05.002

Crouzet, C., Wilhelm, B., Sabatier, P., Demory, F., Thouveny, N., Pignol, C., Reyss, J.-L., Magand, O., Jeltsch-Thömmes, A., Bajard, M., Augustin, L., Arnaud, F., 2019. Palaeomagnetism for chronologies of recent alpine lake sediments: successes and limits. J Paleolimnol 62, 259–278. https://doi.org/10.1007/s10933-019-00087-z

De Putter, T., Loutre, M.-F., Wansard, G., 1998. Decadal periodicities of Nile River historical discharge (A.D. 622–1470) and climatic implications. Geophysical Research Letters 25, 3193–3196. https://doi.org/10.1029/98GL02250

Dereje, H., Daneal, S.F., Yenesew, M., Azage, G.Y., Taddesse, S., Naod, M., Tariku, A., 2018. The Study of Water Use and Treated Wastewater Discharge charge. Report on Charge System for Irrigation Water Abstraction and Use. Federal Democratic Republic of Ethiopia Awash Basin Authority.

Dosio, A., Jones, R.G., Jack, C., Lennard, C., Nikulin, G., Hewitson, B., 2019. What can we know about future precipitation in Africa? Robustness, significance and added value of projections from a large ensemble of regional climate models. Clim Dyn 53, 5833–5858. https://doi.org/10.1007/s00382-019-04900-3

Eltahir, E.A.B., 1996. El Niño and the Natural Variability in the Flow of the Nile River. Water Resour. Res. 32, 131–137. https://doi.org/10.1029/95WR02968

Emerton, R., Cloke, H.L., Stephens, E.M., Zsoter, E., Woolnough, S.J., Pappenberger, F., 2017. Complex picture for likelihood of ENSO-driven flood hazard. Nat Commun 8, 14796. https://doi.org/10.1038/ncomms14796

FAO, 2023. Drought in the Horn of Africa: Progress report on the rapid response and mitigation plan to avert a humanitarian catastrophe (January–December 2022). FAO. https://doi.org/10.4060/cc4218en

FAO, 2022. Drought in the Horn of Africa – Rapid response and mitigation plan to avert a humanitarian catastrophe. FAO. https://doi.org/10.4060/cb8280en
FAO, 2000. The Elimination of Food Insecurity in the Horn of Africa – Summary Report. Rome.
Ficchì, A., Cloke, H., Neves, C., Woolnough, S., Coughlan de Perez, E., Zsoter, E., Pinto, I., Meque, A., Stephens, E., 2021. Beyond El Niño: Unsung climate modes drive African floods. Weather and Climate Extremes 33, 100345. https://doi.org/10.1016/j.wace.2021.100345
Folk, R.L., Ward, W.C., 1957. Brazos River Bar: A Study in the Significance of Grain Size Parameters. Journal Of Sedimentary Petrology 27, 3–26.
Fontaine, R.E., Najjar, A.E., Prince, J.S., 1961. The 1958 malaria epidemic in Ethiopia. Am J Trop Med Hyg 10, 795–803. https://doi.org/10.4269/ajtmh.1961.10.795
Foucher, A., Chaboche, P.-A., Sabatier, P., Evrard, O., 2021. A worldwide meta-analysis (1977–2020) of sediment core dating using fallout radionuclides including ^{137}Cs and $^{210}Pb_{xs}$. Earth System Science Data 13, 4951–4966. https://doi.org/10.5194/essd-13-4951-2021
FSNAU, 2022. Somalia FSNAU Food Security & Nutrition Quarterly Brief — Focus on Post Gu 2017 Season Early Warning (Food Security and Nutrition Analysis Unit and Famine Early Warning System Network, 2022). FSNAU.
Garcia-Gil, S., Vilas, F., Garcia-Garcia, A., 2002. Shallow gas features in incised-valley fills (Ría de Vigo, NW Spain): a case study. Continental Shelf Research 22, 2303–2315. https://doi.org/10.1016/S0278-4343(02)00057-2
Gilli, A., Anselmetti, F.S., Glur, L., Wirth, S.B., 2013. Lake Sediments as Archives of Recurrence Rates and Intensities of Past Flood Events, in: Schneuwly-Bollschweiler, M., Stoffel, M., Rudolf-Miklau, F. (Eds.), Dating Torrential Processes on Fans and Cones: Methods and Their Application for Hazard and Risk Assessment, Advances in Global Change Research. Springer Netherlands, Dordrecht, pp. 225–242. https://doi.org/10.1007/978-94-007-4336-6_15
Grothe, P.R., Cobb, K.M., Liguori, G., Di Lorenzo, E., Capotondi, A., Lu, Y., Cheng, H., Edwards, R.L., Southon, J.R., Santos, G.M., Deocampo, D.M., Lynch-Stieglitz, J., Chen, T., Sayani, H.R., Thompson, D.M., Conroy, J.L., Moore, A.L., Townsend, K., Hagos, M., O'Connor, G., Toth, L.T., 2020. Enhanced El Niño–Southern Oscillation Variability in Recent Decades. Geophysical Research Letters 47, e2019GL083906. https://doi.org/10.1029/2019GL083906
Haberzettl, T., Kirsten, K.L., Kasper, T., Franz, S., Reinwarth, B., Baade, J., Daut, G., Meadows, M.E., Su, Y., Mäusbacher, R., 2019. Using 210Pb-data and paleomagnetic secular variations to date anthropogenic impact on a lake system in the Western Cape, South Africa. Quaternary Geochronology 51, 53–63. https://doi.org/10.1016/j.quageo.2018.12.004
Hersbach, H., Bell, B., Berrisford, P., Hirahara, S., Horányi, A., Muñoz-Sabater, J., Nicolas, J., Peubey, C., Radu, R., Schepers, D., Simmons, A., Soci, C., Abdalla, S., Abellan, X., Balsamo, G., Bechtold, P., Biavati, G., Bidlot, J., Bonavita, M., De Chiara, G., Dahlgren, P., Dee, D., Diamantakis, M., Dragani, R., Flemming, J., Forbes, R., Fuentes, M., Geer, A., Haimberger, L., Healy, S., Hogan, R.J., Hólm, E., Janisková, M., Keeley, S., Laloyaux, P., Lopez, P., Lupu, C., Radnoti, G., de Rosnay, P., Rozum, I., Vamborg, F., Villaume, S., Thépaut, J.-N., 2020. The ERA5 global reanalysis. Quarterly Journal of the Royal Meteorological Society 146, 1999–2049. https://doi.org/10.1002/qj.3803
Hua, Q., Barbetti, M., Rakowski, A.Z., 2013. Atmospheric radiocarbon for the period 1950-2010.

IPCC, 2022. Working Group II contribution to the Sixth Assesment Report of the Intergovernmental Panel on Climate Change.

Jackson, A., Jonkers, A.R.T., Walker, M.R., 2000. Four Centuries of Geomagnetic Secular Variation from Historical Records. Philosophical Transactions: Mathematical, Physical and Engineering Sciences 358, 957–990.

Jackson, M.L., 2005. Soil chemical analysis : advanced course : a manual of methods useful for instruction and research in soil chemistry, physical chemistry of soils, soil fertility, and soil genesis. Parallel Press, University of Wisconsin-Madison Libraries, [2005] ©2005, Revised second edition. Madison, Wis.

Jenny, J.-P., Wilhelm, B., Arnaud, F., Sabatier, P., Giguet Covex, C., Mélo, A., Fanget, B., Malet, E., Ployon, E., Perga, M.E., 2014. A 4D sedimentological approach to reconstructing the flood frequency and intensity of the Rhône River (Lake Bourget, NW European Alps). J Paleolimnol 51, 469–483. https://doi.org/10.1007/s10933-014-9768-4

Kidane, D., Mekonnen, A., Teketay, D., 2014. Contributions of Tendaho Irrigation Project to the Improvement of Livelihoods of Agropastoralists in the Lower Awash Basin, Northeastern Ethiopia. Ethiopian e-journal for research and innovationforesight 6, 1–19.

Kylander, M.E., Ampel, L., Wohlfarth, B., Veres, D., 2011. High-resolution X-ray fluorescence core scanning analysis of Les Echets (France) sedimentary sequence: new insights from chemical proxies. Journal of Quaternary Science 26, 109–117. https://doi.org/10.1002/jqs.1438

Lapointe, F., Francus, P., Lamoureux, S.F., Saïd, M., Cuven, S., 2012. 1750 years of large rainfall events inferred from particle size at East Lake, Cape Bounty, Melville Island, Canada. J Paleolimnol 48, 159–173. https://doi.org/10.1007/s10933-012-9611-8

Lefebvre, P., Sabatier, P., Mangeret, A., Gourgiotis, A., Le Pape, P., Develle, A.-L., Louvat, P., Diez, O., Reyss, J.-L., Gaillardet, J., Cazala, C., Morin, G., 2021. Climate-driven fluxes of organic-bound uranium to an alpine lake over the Holocene. Science of The Total Environment 783, 146878. https://doi.org/10.1016/j.scitotenv.2021.146878

Lennard, C.J., Nikulin, G., Dosio, A., Moufouma-Okia, W., 2018. On the need for regional climate information over Africa under varying levels of global warming. Environ. Res. Lett. 13, 060401. https://doi.org/10.1088/1748-9326/aab2b4

Li, C.-G., Zheng, Y., Wang, M., Sun, Z., Jin, C., Hou, J., 2021. Refined dating using palaeomagnetic secular variations on a lake sediment core from Guozha Co, northwestern Tibetan Plateau. Quaternary Geochronology 62, 101146. https://doi.org/10.1016/j.quageo.2020.101146

MacLeod, D., Caminade, C., 2019. The Moderate Impact of the 2015 El Niño over East Africa and Its Representation in Seasonal Reforecasts. Journal of Climate 32, 7989–8001. https://doi.org/10.1175/JCLI-D-19-0201.1

Martín-Puertas, C., Valero-Garcés, B.L., Mata, M.P., Moreno, A., Giralt, S., Martínez-Ruiz, F., Jiménez-Espejo, F., 2011. Geochemical processes in a Mediterranean Lake: a high-resolution study of the last 4,000 years in Zoñar Lake, southern Spain. Journal of Paleolimnology 46, 405–421. https://doi.org/10.1007/s10933-009-9373-0

Marzin, C., Braconnot, P., 2009. The role of the ocean feedback on Asian and African monsoon variations at 6kyr and 9.5kyr BP. Comptes Rendus Geoscience 341, 643–655. https://doi.org/10.1016/j.crte.2009.09.001

Mera, G.A., 2018. Drought and its impacts in Ethiopia. Weather and Climate Extremes 22, 24–35. https://doi.org/10.1016/j.wace.2018.10.002

Molinaroli, E., Guerzoni, S., De Falco, G., Sarretta, A., Cucco, A., Como, S., Simeone, S., Perilli, A., Magni, P., 2009. Relationships between hydrodynamic parameters and

https://doi.org/10.5194/egusphere-2024-310
Preprint. Discussion started: 5 March 2024

grain size in two contrasting transitional environments: The Lagoons of Venice and Cabras, Italy. Sedimentary Geology 219, 196–207. https://doi.org/10.1016/j.sedgeo.2009.05.013

Mologni, C., Bruxelles, L., Schuster, M., Davtian, G., Ménard, C., Orange, F., Doubre, C., Cauliez, J., Taezaz, H.B., Revel, M., Khalidi, L., 2021. Holocene East African monsoonal variations recorded in wave-dominated clastic paleo-shorelines of Lake Abhe, Central Afar region (Ethiopia & Djibouti). Geomorphology 391, 107896. https://doi.org/10.1016/j.geomorph.2021.107896

Mologni, C., Revel, M., Blanchet, C., Bosch, D., Develle, A.-L., Orange, F., Bastian, L., Khalidi, L., Ducassou, E., Migeon, S., 2020. Frequency of exceptional Nile flood events as an indicator of Holocene hydro-climatic changes in the Ethiopian Highlands. Quaternary Science Reviews 247, 106543. https://doi.org/10.1016/j.quascirev.2020.106543

Mouelhi, S., Michel, C., Perrin, C., Andréassian, V., 2006. Stepwise development of a two-parameter monthly water balance model. Journal of Hydrology 318, 200–214. https://doi.org/10.1016/j.jhydrol.2005.06.014

Murray, H.D., 1975. Melanoides tuberculata (Müller), Las Morras Creek, Bracketville. Bullettin Of The American Malacological Union 1, 43.

Nash, J.E., Sutcliffe, J.V., 1970. River flow forecasting through conceptual models part I — A discussion of principles. Journal of Hydrology 10, 282–290. https://doi.org/10.1016/0022-1694(70)90255-6

Niang, I., Ruppel, O.C., Abdrabo, M.A., Essel, A., Lennard, C., Padgham, J., Urquhart, P., Adelekan, I., Archibald, S., Barkhordarian, A., Battersby, J., Chahed, M., Chatterjee, M., Chidiezie, C.T., Descheemaeker, K., Djoudi, H., Ebi, K.L., Fall, P.D., Fuentes, R., Garland, R., Harvey, B., Hayden, M., Hemp, A., Jobbins, G., Johnson, J., Lobell, D., Locatelli, B., Ludi, E., Naess, L.O., Ndebele-Murisa, M.R., Ndiaye, A., Newsham, A., Njai, S., Pauw, P., Pramova, E., Rakotondrafara, M.-L., Raleigh, C., Roberts, D., Schleyer, M.H., Victor, D., Vincent, K., Dube, P., Leary, N., Schulte-Uebbing, L., 2014. Part B: Regional Aspects. Contribution of Working Group II to the Fifth Assessment Report of the Intergovernmental Panel on Climate Change - Africa, in: Climate Change 2014: Impacts, Adaptation, and Vulnerability., Cambridge University Press. Cambridge, United Kingdom and New York, NY, USA, pp. 1199–1265.

Nicholson, S.E., 2017. Climate and climatic variability of rainfall over eastern Africa. Reviews of Geophysics 55, 590–635. https://doi.org/10.1002/2016RG000544

OCHA, 2022. Horn of Africa Drought: Regional Humanitarian Overview & Call to Action. OCHA.

Ólafsdóttir, S., Geirsdóttir, Á., Miller, G.H., Stoner, J.S., Channell, J.E.T., 2013. Synchronizing Holocene lacustrine and marine sediment records using paleomagnetic secular variation. Geology 41, 535–538. https://doi.org/10.1130/G33946.1

Oudin, L., Hervieu, F., Michel, C., Perrin, C., Andréassian, V., Anctil, F., Loumagne, C., 2005. Which potential evapotranspiration input for a lumped rainfall–runoff model?: Part 2—Towards a simple and efficient potential evapotranspiration model for rainfall–runoff modelling. Journal of Hydrology 303, 290–306. https://doi.org/10.1016/j.jhydrol.2004.08.026

Palmer, P.I., Wainwright, C.M., Dong, B., Maidment, R.I., Wheeler, K.G., Gedney, N., Hickman, J.E., Madani, N., Folwell, S.S., Abdo, G., Allan, R.P., Black, E.C.L., Feng, L., Gudoshava, M., Haines, K., Huntingford, C., Kilavi, M., Lunt, M.F., Shaaban, A., Turner, A.G., 2023. Drivers and impacts of Eastern African rainfall variability. Nat Rev Earth Environ 4, 254–270. https://doi.org/10.1038/s43017-023-00397-x

https://doi.org/10.5194/egusphere-2024-310
Preprint. Discussion started: 5 March 2024

Parris, A.S., Bierman, P.R., Noren, A.J., Prins, M.A., Lini, A., 2010. Holocene paleostorms identified by particle size signatures in lake sediments from the northeastern United States. J Paleolimnol 43, 29–49. https://doi.org/10.1007/s10933-009-9311-1

Pekel, J.-F., Cottam, A., Gorelick, N., Belward, A.S., 2016. High-resolution mapping of global surface water and its long-term changes. Nature 540, 418–422. https://doi.org/10.1038/nature20584

Rauch, S., Hemond, H.F., Brabander, D.J., 2006. High spatial resolution analysis of lake sediment cores by laser ablationinductively coupled plasma-mass spectrometry (LA-ICP-MS): Lake sediment cores by laser ablation-ICP-MS. Limnol. Oceanogr. Methods 4, 268–274. https://doi.org/10.4319/lom.2006.4.268

Reyss, J.-L., Schmidt, S., Legeleux, F., Bonté, P., 1995. Large, low background well-type detectors for measurements of environmental radioactivity. Nuclear Instruments and Methods in Physics Research Section A: Accelerators, Spectrometers, Detectors and Associated Equipment 357, 391–397. https://doi.org/10.1016/0168-9002(95)00021-6

Roussel, E.G., Sauvadet, A.-L., Allard, J., Chaduteau, C., Richard, P., Bonavita, M.-A.C., Chaumillon, E., 2009. Archaeal Methane Cycling Communities Associated with Gassy Subsurface Sediments of Marennes-Oléron Bay (France). Geomicrobiology Journal 26, 31–43. https://doi.org/10.1080/01490450802599284

Sabatier, P., Moernaut, J., Bertrand, S., Van Daele, M., Kremer, K., Chaumillon, E., Arnaud, F., 2022. A Review of Event Deposits in Lake Sediments. Quaternary 5, 34. https://doi.org/10.3390/quat5030034

Sabatier, P., Wilhelm, B., Ficetola, G.F., Moiroux, F., Poulenard, J., Develle, A.-L., Bichet, A., Chen, W., Pignol, C., Reyss, J.-L., Gielly, L., Bajard, M., Perrette, Y., Malet, E., Taberlet, P., Arnaud, F., 2017. 6-kyr record of flood frequency and intensity in the western Mediterranean Alps – Interplay of solar and temperature forcing. Quaternary Science Reviews 170, 121–135. https://doi.org/10.1016/j.quascirev.2017.06.019

Schiefer, E., Gilbert, R., Hassan, M.A., 2011. A lake sediment-based proxy of floods in the Rocky Mountain Front Ranges, Canada. J Paleolimnol 45, 137–149. https://doi.org/10.1007/s10933-010-9485-6

Slivinski, L.C., Compo, G.P., Whitaker, J.S., Sardeshmukh, P.D., Giese, B.S., McColl, C., Allan, R., Yin, X., Vose, R., Titchner, H., Kennedy, J., Spencer, L.J., Ashcroft, L., Brönnimann, S., Brunet, M., Camuffo, D., Cornes, R., Cram, T.A., Crouthamel, R., Domínguez-Castro, F., Freeman, J.E., Gergis, J., Hawkins, E., Jones, P.D., Jourdain, S., Kaplan, A., Kubota, H., Blancq, F.L., Lee, T.-C., Lorrey, A., Luterbacher, J., Maugeri, M., Mock, C.J., Moore, G.W.K., Przybylak, R., Pudmenzky, C., Reason, C., Slonosky, V.C., Smith, C.A., Tinz, B., Trewin, B., Valente, M.A., Wang, X.L., Wilkinson, C., Wood, K., Wyszyński, P., 2019. Towards a more reliable historical reanalysis: Improvements for version 3 of the Twentieth Century Reanalysis system. Quarterly Journal of the Royal Meteorological Society 145, 2876–2908. https://doi.org/10.1002/qj.3598

Spencer, T., Laughton, A.S., Flemming, N.C., Black, E., 2005. The relationship between Indian Ocean sea–surface temperature and East African rainfall. Philosophical Transactions of the Royal Society A: Mathematical, Physical and Engineering Sciences 363, 43–47. https://doi.org/10.1098/rsta.2004.1474

Syvitski, J., Ángel, J.R., Saito, Y., Overeem, I., Vörösmarty, C.J., Wang, H., Olago, D., 2022. Earth's sediment cycle during the Anthropocene. Nat Rev Earth Environ 3, 179–196. https://doi.org/10.1038/s43017-021-00253-w

Taddese, G., Sonder, K., Peden, D., 2010. THE WATER OF THE AWASH RIVER BASIN A FUTURE CHALLENGE TO ETHIOPIA. report 14.

Varet, J., 2018. Geology of Afar (East Africa), Springer. ed, Regional Geology Reviews.

https://doi.org/10.5194/egusphere-2024-310
Preprint. Discussion started: 5 March 2024

Wang, G., Eltahir, E.A.B., 1999. Use of ENSO Information in Medium- and Long-Range Forecasting of the Nile Floods. Journal of Climate 12, 1726–1737. https://doi.org/10.1175/1520-0442(1999)012<1726:UOEIIM>2.0.CO;2

Ward, P.J., Eisner, S., Flörke, M., Dettinger, M.D., Kummu, M., 2014. Annual flood sensitivities to El Niño–Southern Oscillation at the global scale. Hydrology and Earth System Sciences 18, 47–66. https://doi.org/10.5194/hess-18-47-2014

WBG, 2018. Somalia Drought Impact and Needs Assessment: Synthesis Report (World Bank Group, 2018). World Bank Group.

Webster, P.J., Moore, A.M., Loschnigg, J.P., Leben, R.R., 1999. Coupled ocean-atmosphere dynamics in the Indian Ocean during 1997-98. Nature 401, 356–360. https://doi.org/10.1038/43848

Weltje, G.J., Tjallingii, R., 2008. Calibration of XRF core scanners for quantitative geochemical logging of sediment cores: Theory and application. Earth and Planetary Science Letters 274, 423–438. https://doi.org/10.1016/j.epsl.2008.07.054

Wilhelm, B., Arnaud, F., Sabatier, P., Crouzet, C., Brisset, E., Guiter, F., Reyss, J.L., Chaumillon, E., Tachikawa, K., Bard, E., Delannoy, J.J., 2012. 1.4 kyrs of flash flood events in the Southern European Alps: implications for extreme precipitation patterns and forcing over the north-western Mediterranean area 9097.

Wilhelm, B., Ballesteros Canovas, J.A., Corella Aznar, J.P., Kämpf, L., Swierczynski, T., Stoffel, M., Støren, E., Toonen, W., 2018. Recent advances in paleoflood hydrology: From new archives to data compilation and analysis. Water Security 3, 1–8. https://doi.org/10.1016/j.wasec.2018.07.001

Wilhelm, B., Rapuc, W., Amann, B., Anselmetti, F.S., Arnaud, F., Blanchet, J., Brauer, A., Czymzik, M., Giguet-Covex, C., Gilli, A., Glur, L., Grosjean, M., Irmler, R., Nicolle, M., Sabatier, P., Swierczynski, T., Wirth, S.B., 2022. Impact of warmer climate periods on flood hazard in the European Alps. Nat. Geosci. 15, 118–123. https://doi.org/10.1038/s41561-021-00878-y

Wilhelm, B., Sabatier, P., Arnaud, F., 2015. Is a regional flood signal reproducible from lake sediments? Sedimentology 62, 1103–1117. https://doi.org/10.1111/sed.12180

Yemane, W., 2008. Challenges and Prospects of Commercial Agriculture Entreprise Development and the Afar Pastoralists: The Case of Tendaho Dam and Irrigation Project. Addis Ababa University, Addis Ababa.

Zaroug, M.A.H., Eltahir, E.A.B., Giorgi, F., 2014. Droughts and floods over the upper catchment of the Blue Nile and their connections to the timing of El Niño and La Niña events. Hydrol. Earth Syst. Sci. 18, 1239–1249. https://doi.org/10.5194/hess-18-1239-2014